



1 **EcoTWIN 1.0: A Fully Distributed Tracer-Aided Ecohydrological Model Tracking Water,**  
2 **Isotopes, and Nutrients**

3 Songjun Wu<sup>1</sup>, Doerthe Tetzlaff<sup>1,2</sup>, Yi Zheng<sup>3</sup>, Chris Soulsby<sup>4</sup>

4 1 Department of Ecohydrology and Biogeochemistry, Leibniz Institute of Freshwater Ecology and  
5 Inland Fisheries, Berlin, Germany

6 2 Geography Institute and IRI THESys, Humboldt University of Berlin, Berlin, Germany

7 3 School of Environmental Science and Engineering, Southern University of Science and Technology,  
8 Shenzhen, China

9 4 Northern Rivers Institute, School of Geosciences, University of Aberdeen, UK

10 Corresponding author: Songjun Wu ([songjun.wu@igb-berlin.de](mailto:songjun.wu@igb-berlin.de))

11

12 **Abstract**

13 The value of stable water isotopes in constraining process representation in hydrological models is  
14 well acknowledged with numerous tracer-aided hydrological models developed in recent years, yet  
15 few have leveraged these benefits for more robust water quality modelling. Therefore, we introduce  
16 EcoTWIN, a fully distributed tracer-aided *ecohydrological* model that simultaneously **tracks water,**  
17 **isotopic,** and **nutrient** fluxes in an integrated C++ framework. A thorough validation was conducted by  
18 calibrating EcoTWIN against discharge, in-stream isotopes, and NO<sub>3</sub>-N concentrations (1980-2024) in  
19 17 large-scale (10<sup>3</sup> - 10<sup>5</sup> km<sup>2</sup>) European catchments spanning a wide range of geographic and climatic  
20 gradients. Furthermore, three reanalysis products (ERA5 snow depth, MODIS evapotranspiration, and  
21 GRACE surface water anomaly) were employed to further validate the capacity of EcoTWIN to  
22 reproduce associated internal water fluxes without calibration. Results showed good model  
23 performance of both calibrated in-stream targets and uncalibrated internal fluxes in most catchments.  
24 Therefore, we conclude that EcoTWIN is a flexible, transferable modelling tool for prediction and  
25 process inference in terrestrial ecosystems ranging from boreal to subtropic climates. Constrained by  
26 tracer simulations, the model not only captures the celerity, but also the velocity of hydrological fluxes,  
27 thus providing spatio-temporally-explicit estimations of water ages and travel times. Such information  
28 provides opportunities to bridge catchment hydrology and water quality by linking travel times with  
29 biogeochemical processing times. We demonstrate this with a proof of concept using Damköhler  
30 Number in nitrogen modelling.

31

32 **1 Introduction**

33 The development of ecohydrological models has been accelerating in the recent decades towards  
34 frameworks that are more distributed (instead of lumped or semi-distributed) and complex  
35 (integrating more ecohydrological processes) (Pechlivanidis et al., 2011; Wellen et al., 2015). A few  
36 examples include SWAT (Arnold et al., 2012), HYPE (Lindström et al., 2010), and mHM-Nitrate (Yang  
37 et al., 2018), which have been widely applied worldwide. As process-based models, they are used not



38 only as prediction tools for specific variables, but also as learning tools for model inference, i.e., to  
39 track the internal states/fluxes from available observations (Wang et al., 2024). This, however, poses  
40 challenges.

41 Inference of internal processes is naturally uncertain due to the lack of direct observations, though  
42 such uncertainty can be somehow constrained by rigorous split-sample calibration and validation. The  
43 reason we use “somehow” here is based on the fact that most models are calibrated to a minimal  
44 number of variables, and 81% of calibrations used data from a single gauge (mostly at a catchment  
45 outlet) as reviewed in Wellen et al., (2015). Additionally, from a technical perspective, “equifinality”  
46 further adds to the inference uncertainty due to the potential misinformation in data (uncertainty in  
47 model forcing and observations) and model structure (the use of simplified, abstract mathematics to  
48 simulate real world processes) (Beven, 2006). This can result in inaccurate process representations  
49 yielding deceptively good results through error compensation, thus leading to overconfidence in a  
50 model's ability to reproduce within-basin dynamics (Wen et al., 2024; Wu et al., 2025a). As  
51 acknowledged by the hydrological community, models calibrated solely against discharge at the  
52 catchment outlet reflect only the celerity of hydrological systems (pressure wave propagation), yet  
53 constituent transport in water quality modelling relies on the velocity (mass flux of the water)  
54 (McDonnell & Beven, 2014). Failure to reconcile these differences can lead to questionable process  
55 inferences from many ecohydrological and water quality models.

56 One way to strengthen model inference is to include auxiliary data for calibration (Efstratiadis &  
57 Koutsoyiannis, 2010). However, there is a paradox in multi-criteria calibration, as on the one hand,  
58 more auxiliary data will feed unique information to the calibration process, thus effectively  
59 constraining the model behaviour from an ecohydrological perspective; yet on the other hand, it  
60 increases the dimensionality of calibration thus resulting in degraded performance or failure of  
61 calibration from a technical perspective. The “curse” of dimensionality in ecohydrological modelling is  
62 universal for all the commonly used algorithms under both Bayesian and Pareto theories as  
63 demonstrated in Wu et al., (2025c). Therefore, modellers should expect the selected auxiliary data to  
64 contain as much information as possible (Nearing et al., 2020). For distributed modelling, the auxiliary  
65 data should reflect the cumulative contribution of all upstream reaches/regions, rather than variables  
66 that are highly dependent on local condition/processes (e.g. point-scale soil moisture and  
67 evapotranspiration measurements etc.).

68 Stable water isotopes, in this context, have powerful potential in cumulative flux tracking. As  
69 conservative tracers,  $^2\text{H}$  and  $^{18}\text{O}$  are independent of biogeochemical reactions and naturally integrate  
70 landscape heterogeneity, thus providing effective constraints on spatially distributed (dis)connections  
71 of hydrological flow paths as well as velocity of the hydrological systems which reflect flux-storage  
72 interactions (Jung et al., 2025; Tetzlaff et al., 2015). The value of tracers has long been recognised by  
73 hydrologists (Hooper et al., 1988), with many tracer-aided hydrological models developed and evolved  
74 in recent years from lumped (Birkel et al., 2011; Godsey et al., 2010), to semi-distributed (van  
75 Huijgevoort et al., 2016; Nan et al., 2021), and distributed structure (Kuppel et al., 2018; Remondi et  
76 al., 2018). However, few attempts have been made to integrate a tracer-aided hydrological structure



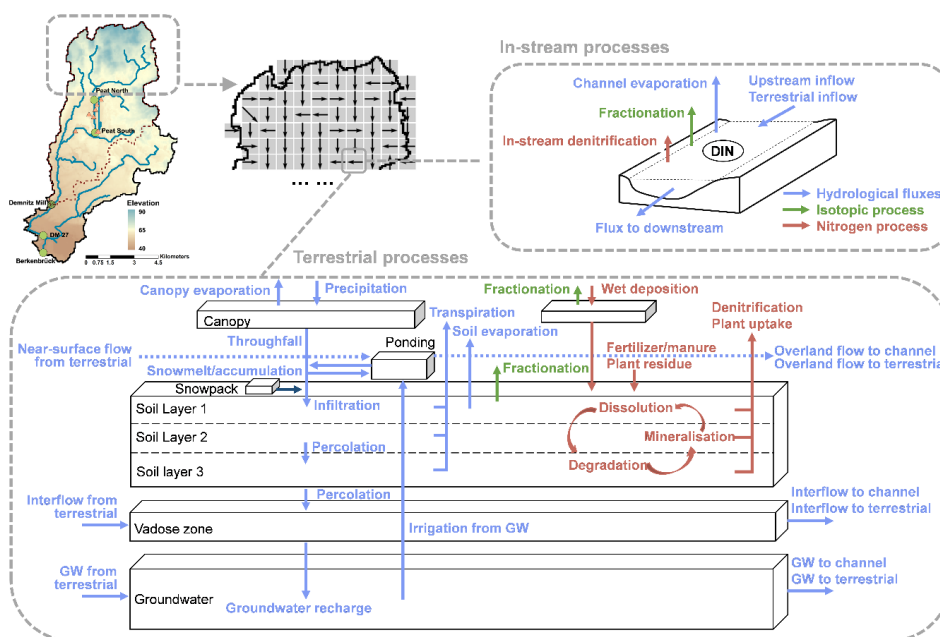
77 into water quality modelling (Birkel & Soulsby, 2015; Jung et al., 2025), despite the need being evident  
78 for nearly four decades (Neal et al., 1988). Moreover, existing pioneering models are mostly  
79 conceptualised/lumped (Benettin et al., 2015; Dick et al., 2015) and/or loosely coupled via external  
80 tracer/water quality modules (Pesántez et al., 2023; Yang et al., 2024; Zhang et al., 2020). The external  
81 coupling of model chains transfer necessary internal states and fluxes between sub-models (e.g.  
82 hydrological fluxes for constituent mixing in water quality or isotopic modules) on disk (instead of  
83 memory), thus significantly increasing the resources consumption in input/output operations. Such  
84 model chains, though provide useful scientific insights, can become problematic for large-scale  
85 applications owing to the exponential growth in computational and storage requirements. Therefore,  
86 there remains a need to develop a fully distributed, computationally efficient ecohydrological model  
87 that combines hydrological, isotopic, and water quality simulations.

88 This research gap motivated the development of EcoTWIN, the model that we present in this paper.  
89 To our knowledge, the model is one of the first distributed tracer-aided *ecohydrological* models that  
90 **tracks water, isotopic, and nutrient** fluxes simultaneously in an integrated C++ framework. For a  
91 thorough testing of EcoTWIN, 17 large European catchments were selected for calibration against  
92 discharge, in-stream isotopes, and NO<sub>3</sub>-N concentrations. These catchments span over a wide range  
93 of geographic (Alpine to lowland plain) and climatic (from snow-dominated to Mediterranean)  
94 gradients. In addition, the robustness of modelled inference on uncalibrated internal fluxes were also  
95 compared with three remote sensing products (snow depth, evapotranspiration, and water storage).  
96 Given the overall good integrated performance in most catchments, EcoTWIN is presented as an  
97 ecohydrological modelling framework applicable for terrestrial ecosystems ranging from boreal to  
98 temperate and subtropical climates across a wide range of geographical environments. The  
99 subsequent sections are organised as follows: Section 2 and 3 introduce the model structure of  
100 EcoTWIN and details in calibration and validation; the model performance is shown in Section 4; in  
101 Section 5 we show the advantages of a tracer-aided ecohydrological framework with an example of  
102 how water ages bridge catchment hydrology and water quality models; finally, the current limitations  
103 and planned future development of EcoTWIN are also discussed.

104

## 105 **2 Model description**

106 EcoTWIN is fully distributed ecohydrological model implemented in C++. The model consists of  
107 hydrological, isotopic, and nitrogen modules, which simulate major ecohydrological states and fluxes  
108 from canopy to groundwater (Figure 1). Aided with tracer simulation, the model is additionally able to  
109 track the water movement vertically and laterally via the calculation of water ages and travel times.  
110 For detailed information of model parameters please refer to Table S1.



111

112 Figure 1. Model structure of EcoTWIN.

113

## 114 2.1 Hydrological module

115 EcoTWIN follows a typical multi-layer, top-down, bucket-type approach that resolves the water  
 116 balance sequentially for the vegetation canopy, three soil layers, vadose zone, and groundwater. As  
 117 the foundation of solute transport, the hydrological module employs a selective disassembly structure  
 118 with multiple alternative conceptualisations possible for specific important hydrological processes.  
 119 The configuration can be specified *a priori* based on the goal of modelling and prior knowledge of the  
 120 studied catchment(s).

### 121 2.1.1 Soil properties

122 Before iterative simulations, soil characteristics are estimated using appropriate pedotransfer  
 123 functions. Three different alternatives are provided, each of which requires different levels of inputs  
 124 but all were found to provide robust estimation of soil porosity ( $\theta_s$ ), field capacity ( $\theta_{fc}$ ), wilting point  
 125 ( $\theta_{wp}$ ), and hydraulic conductivity ( $K_s$ ). All the soil properties are required for each soil layer/depth.  
 126 This can be achieved via three alternative options: (i) assigning identical properties across the whole  
 127 soil column, (ii) calculating separately for each depth based on depth-dependent inputs, or (iii)  
 128 extrapolating deeper profile characteristics from the top soil properties based on a depth-dependent  
 129 equation in Maneta & Silverman, (2013).



130 The distribution of soil types and land use are assigned from raster file in EcoTWIN. This can be  
131 specified as a static boundary condition; alternatively, the distributions can also be updated  
132 dynamically via a user-specified interval to reflect any temporal changes due to land management.

133

### 134 **2.1.2 Vertical fluxes**

135 The vertical fluxes are resolved for storages in the canopy, soil layers, vadose zone, and groundwater.  
136 The mass balance of canopy storage ( $\Delta C$ ) follows:

$$\Delta C = P - I - Th \quad (1)$$

137 where  $P$ ,  $I$ ,  $Th$  are precipitation, interception, and throughfall, respectively. The throughfall is  
138 calculated as the exceedance of current canopy storage from the maximum storage calculated by Leaf  
139 Area index  $LAI$  and a correlation parameter  $\alpha$ .

$$C_{max} = \alpha * LAI \quad (2-1)$$

140 Alternatively, the maximum canopy storage can be estimated with explicit consideration of  
141 precipitation intensity (Landgraf et al., 2023):

$$C_{max} = \alpha * LAI * \left(1 - \frac{1}{1 + SCF * P / (\alpha * LAI)}\right) \quad (2-2)$$

142 where  $SCF$  is the vegetation cover fraction calculated by  $LAI$  and an extinction coefficient ( $rE$ )  
143 adopted from HYDRUS-1D (Šimůnek et al., 2013):

$$SCF = 1 - \exp(rE * LAI) \quad (3)$$

144 Then throughfall is calculated as the exceedance of canopy storage from the maximum:

$$Th = (P + C) - C_{max} \text{ if } (P + C) > C_{max} \text{ else } 0 \quad (4)$$

145 After reaching land surface, throughfall becomes ponding water ( $S_{Pond}$ ) or snow ( $S_{snow}$ ) depending  
146 on a temperature threshold for separation ( $Thre_{SN}$ ). Snow will melt and recharge the ponding water  
147 in warm conditions (air temperature  $Ta$  exceed  $Thre_{SN}$ ) following a degree-day model.

$$melt = S_{snow} * \min(dd_{min} + dd_{inc} * Th * (Ta - Thre_{SN}), dd_{max}) \quad (5)$$

148 Where  $dd_{min}$  and  $dd_{max}$  are the minimum and maximum of degree day factor, while  $dd_{inc}$  denotes  
149 the rate of increase in the degree-day factor per degree Celsius rise in temperature.

150 The available ponding water infiltrates into the top soil layer using Green-Ampt model (Kale & Sahoo,  
151 2011; Maneta & Silverman, 2013), with infiltration capacity first calculated as a function of average  
152 soil moisture over the hydrologically active depth:

$$I_f = Ks * \left(1 + \frac{\psi * \theta_s * (1 - (\theta_1 - \theta_{wt}) / (\theta_s - \theta_{wt}))}{\theta_1 * d_1}\right) \quad (6)$$

153 Where  $\theta_1$ ,  $\theta_s$ ,  $\theta_{wt}$ , and  $d_1$  are the moisture content, porosity, wilting point, and depth in top soil layer;  
154  $\psi$  is a parameter representing soil air entry pressure in m. Then potential infiltration ( $F_p$ ) is determined



155 from the lesser between the available ponding water ( $S_{pd}$ ) and potential infiltration rate integrated  
 156 over time before ponding occurs ( $I_f * t_p$ ).

157 The actual infiltration ( $F$ ) is solved iteratively using the Newton–Raphson scheme:

$$F = \Delta\theta * d_1 = F_p + K_s * w_{Ks} * (\Delta t - t_p) - \psi\Delta\theta * \ln\left(\frac{\psi\Delta\theta + \Delta\theta d_1}{\psi\Delta\theta + F_p}\right) \quad (7)$$

158 where  $w_{Ks}$  is anisotropy ratio of vertical to horizontal  $K_s$ .

159 The soil storage in each layer is conceptualised as two water pools – a gravitational, free-flowing pool  
 160 and a capillary, soil-bound pool. The two pools are separated based on field capacity (Maneta &  
 161 Silverman, 2013), and percolation happens when soil storage exceeds the threshold. Three alternative  
 162 schemes are included in EcoTWIN.

163 In the first scheme, all water in excess of field capacity percolates to deeper layer:

$$Pc_i = (\theta_i - \theta_{fc}) * d_i \quad (8-1)$$

164 where  $Pc_i$ ,  $\theta_i$  and  $d_i$  depict the percolation, moisture content and depth from/in  $i$ th soil layer in m.

165 The second scheme additionally considers the hydraulic conductivity ( $K_s$ ) following the  
 166 conceptualisation in SWAT (Arnold et al., 2012):

$$Pc_i = (\theta_i - \theta_{fc,i}) * d_i * (1 - \exp\left(\frac{-\Delta t * K_s}{\theta_{s,i} - \theta_{fc,i}}\right)) \quad (8-2)$$

167 The third scheme relates percolation to the extent of soil saturation with an exponential parameter  $\beta$   
 168 (Kumar et al., 2013; Samaniego et al., 2010):

$$Pc_i = (\theta_i - \theta_{fc,i}) * d_i * (1 - \exp(\beta * \log(\theta_i/\theta_{s,i}))) \quad (8-3)$$

169 For evapotranspiration, soil evaporation and transpiration are estimated separately. The separation  
 170 of  $PET$  is realised by surface cover fraction introduced above:

$$PT = PET * SCF; \quad PE = PET - PT \quad (9)$$

171 Soil evaporation is simulated in the top soil layer based on the soil saturation:

$$Evap_s = PE * \min\left(\frac{\theta_1}{\theta_{fc,1}}, 1\right) \quad (10)$$

172 Transpiration is simulated in all soil layers based on the fractions ( $f_{root,i}$ ) of root density ( $D_{root,i}$ ) in  
 173 each layer partitioned by soil depth and a parameter ( $\gamma_{root}$ ):

$$Tr_i = PT * f_{root,i} * \frac{\theta_1 - \theta_{wp,1}}{\theta_{fc,1} - \theta_{wp,1}} \quad (11)$$

$$f_{root,i} = D_{root,i} / \sum_{j=1}^m D_{root,j} \quad (12)$$



$$D_{root,i} = \left(1 - \gamma_{root} \left(\sum_{j=1}^m d_j\right)\right) - \left(1 - \gamma_{root} \left(\sum_{j=1}^i d_j\right)\right) \quad (13)$$

174 Channel evaporation is also estimated using Penman equation, which relies on net radiation, wind  
175 speed, air pressure, and air temperature as inputs.

176 The last soil layer percolates to an unsaturated storage in vadose zone ( $S_{vadose}$ ). The compartment  
177 stores the excess water from soil and percolates either downward to groundwater storage ( $S_{GW}$ ) or  
178 laterally downstream. The percolation to groundwater  $P_{CGW}$  is determined by a weighting parameter  
179  $p_{GW}$  as a proportion of vadose storage:

$$P_{CGW} = S_{vadose} * p_{GW} \quad (14)$$

180 Additionally, irrigation is conceptualised in EcoTWIN, which is realised via the water extraction from  
181 river or groundwater. The source is determined by the geographic location: for a grid cell with channel  
182 network, water is extracted directly from river, and local groundwater is used as irrigation source for  
183 non-channel grids. The amount of extraction is estimated from a predefined coefficient for crop water  
184 demands ( $w_{irr}$ ) from which the deficit is calculated for each of the  $m$  soil layers.

$$deficit = \sum_{i=1}^m (\theta_{fc,i} - \theta_{wp,i}) * w_{irr} * d_i \quad (15)$$

185 Note that the irrigation can switch to groundwater extraction if river storage cannot fill the deficit.

186

### 187 **2.1.3 Lateral fluxes**

188 In EcoTWIN, grid cells are connected laterally at three levels - surface, vadose, and groundwater. Note  
189 that some models omit the vadose/unsaturated storage and directly calculate excess water to drain  
190 based on the saturation extent of the bottom soil layer (e.g., ECH2O-iso, Kuppel et al., 2018). EcoTWIN  
191 did not follow this conceptualisation because in reality, the lateral drainage is focused in the saturated  
192 zone, and thus the bottom of the soil layer instead of the whole soil profile. The drainage of an entire  
193 soil layer thus brings considerable uncertainty to the velocity of lateral transport when the lower  
194 boundary of the soil is a parameter to tune in calibration. For instance, a large soil depth will  
195 dramatically reduce the velocity of interflow drainage and slow down the mixing of constituents,  
196 though this might still perfectly reproduce the celerity (hydrograph) for purely hydrological modelling.  
197 Our conceptualisation (an independent unsaturated compartment) aligns with most hydrological  
198 models (Arnold et al., 2012; Yang et al., 2018) and fits the recent analysis supporting the dominant  
199 role of lateral drainage over vertical transports globally (McMillan et al., 2025).

200 By the end of each timestep, ponding water receives upstream inputs and contributes to channel  
201 storage:

$$Ovf_C = (Ovf_{T,in} + S_{pond}) * p_{Ovf} * dx_C/dx_T \quad (16)$$



202  $dx_C$  and  $dx_T$  are the channel length and size of terrestrial grid cell;  $p_{Ovf}$  is a weighting parameter for  
 203 channel recharge. Then the remaining ponding water routes to downslope terrestrial grid following  
 204 the topographic gradient.

$$Ovf_{T,out} = (Ovf_{T,in} + S_{pond}) - Ovf_C \quad (17)$$

205 Similarly, vadose storage contributes first to channel storage:

$$Inf_C = (Inf_{T,in} + S_{vadose}) * K_{vadose} * \left(1 - e^{-1 * exp_{Inf} * (Inf_{T,in} + S_{vadose})}\right) * p_{Inf} \quad (18)$$

206 where  $K_{vadose}$  is the effective conductivity of lateral transport in the vadose zone; while  $exp_{Inf}$  is an  
 207 exponential parameter determining the strength of positive correlation between recharge and current  
 208 vadose storage. Then the remaining vadose storage is partially routed to downslope grid cell following  
 209 a linear approximation of Kinematic wave equation, which assumes gravitational flux per unit width  
 210  $Inf_{T,out}$  is proportional to the subsurface hydraulic conductivity ( $K_{vadose}$ ) and bedrock slope ( $slope$ )  
 211 approximated from the surface slope):

$$Inf_{T,out} = (Inf_{T,in} + S_{vadose} - Inf_C) * \left(1 + \alpha * \frac{dt}{dx}\right) * \alpha * \frac{dt}{dx} \quad (19)$$

$$\text{where } \alpha = K_{vadose} * \sin(slope)$$

212 Groundwater routing is similar to that of interflow, with channel recharge followed by terrestrial  
 213 transport. Note that the terrestrial groundwater flow does not consider the bedrock slope as  
 214 groundwater storage is generally much large than vadose storage, and thus independent from  
 215 topographic gradients:

$$GWf_C = (GWf_{T,in} + S_{GW}) * K_{GW} * \left(1 - e^{-1 * exp_{GWf} * (GWf_{T,in} + S_{GW})}\right) * p_{GWf} \quad (20)$$

$$GWf_{T,out} = (GWf_{T,in} + S_{GW} - GWf_C) * \left(1 + \alpha * \frac{dt}{dx}\right) * \alpha * \frac{dt}{dx} \quad (21)$$

$$\text{where } \alpha = K_{vadose}$$

216 The channel routing is realised using Kinematic wave equation based on a scaled channel roughness  
 217 parameter (Maneta & Silverman, 2013).

218

## 219 **2.2 Isotopic module**

220 The isotopic module in EcoTWIN tracks the composition of stable water isotopes in all water storage  
 221 compartments following hydrological mixing and fractionation. The module also provides estimation  
 222 of water age and travel time conceptualised as the time since water molecules enter the catchment  
 223 as precipitation, and the time water molecules need to travel through the specific storage.

### 224 **2.2.1 Mixing**

225 The mixing and transport of isotopes ( $^2\text{H}$  and  $^{18}\text{O}$ , both noted as  $C$ ) are governed by the velocity of  
 226 hydrological fluxes with a complete mixing strategy for most water storages:



$$\frac{d(V * C)}{dt} = \sum_{k=1}^{N_{in}} q_{in,k} * C_{in,k} - \sum_{k=1}^{N_{out}} q_{out,k} * C \quad (22)$$

227 Where  $V$  and  $C$  are the volume and composition/concentration of the storage, while  $N_{in}$  and  $N_{out}$   
 228 denote the number of influx and outflux. Such strategy is built on two assumptions: (i) constitutes (i.e.,  
 229 isotopes) are fully mixing within each timestep; (ii) the composition/concentration in outflow equals  
 230 to that in storage. Additional mixing between ponding and upper soil water storage is allowed (with  
 231 proportion determined by a parameter  $SrfMixing$ ), as nutrients in top soils can be flushed out in  
 232 large hydrological events (Seybold et al., 2022).

233 The full-mixing assumptions have been widely used and shown to be reasonable for storages with  
 234 relatively small volumes in many mixing/water quality models (Arnold et al., 2012; Yang et al., 2018).  
 235 However, some studies show that a complete mixing strategy can be problematic for large storages  
 236 such as groundwater (e.g. Soulsby et al., 2015). Therefore, the mass conservation equation used in  
 237 the INCA-N model and mHM-Nitrate is employed to calculated the mixing of groundwater storages  
 238 with influxes (i.e., percolation from vadose storage and lateral groundwater inflow).

$$\frac{dC}{dt} = \frac{1}{V + V_r} * \left( \sum_{k=1}^{N_{in}} q_{in,k} * C_{in,k} - \sum_{k=1}^{N_{out}} q_{out,k} * C \right) \quad (23)$$

239 where  $V_r$  is the retention storage. The equation is solved by the fourth order Runge-Kutta technique.

240

### 241 **2.2.2 Fractionation**

242 As conservative tracers, composition of isotopes in water storages/fluxes is only regulated by kinetic  
 243 fractionation apart from hydrological mixing. The process is accompanied by evaporation, resulting in  
 244 the preferential loss of lighter isotopes ( $^1\text{H}$  and  $^{16}\text{O}$ ) to the vapor phase and a corresponding  
 245 enrichment of heavier isotopes ( $^{18}\text{O}$  and  $^2\text{H}$ ) in the residual water. In EcoTWIN, the fractionation is  
 246 simulated along with evaporation of top soil water and river storage based on the Craig-Gordon model  
 247 (Craig et al., 1964; Kuppel et al., 2018), while transpiration is assumed to be a non-fractionating  
 248 process (Dawson & Ehleringer, 1991; Kuppel et al., 2018).

$$C = C^* - (C^* - C) * \left( \frac{S - Evap}{S} \right)^m \quad (24)$$

249 where  $C^*$  and  $m$  are the limiting isotopic composition (in ‰) and the dimensionless enrichment slop  
 250 that are estimated via the following equations in (Good et al., 2014):

$$C^* = \frac{h_a C_a + h_s \varepsilon^+ + \varepsilon^k}{h_s - h_a + \varepsilon^k / 1000} \quad (25)$$

$$m = \frac{h_a - (h_s \varepsilon^+ + \varepsilon^k) / 1000}{h_s - h_a + \varepsilon^k / 1000} \quad (26)$$



251 where  $h_a$  is the relative humidity above the soil surface normalised from atmospheric relative  
252 humidity ( $h$ ), air temperature ( $T_a$ ), and soil temperature ( $T_s$  estimated from Amato & Giménez, 2024).  
253  $C_a$  is the isotopic composition of ambient air moisture estimated from precipitation composition:

$$C_a = (C_{rain} - \varepsilon^+) / \alpha^+ \quad (27)$$

254 where  $\varepsilon^+$  is the equilibrium fractionation factor (Skrzypek et al., 2015);  $\alpha^+$  is a temperature factor  
255 estimated from  $T_a$ .

$$\varepsilon^+ = (1 - 1/\alpha^+) * 1000 \quad (28)$$

256 The factor of diffusion-controlled kinetic isotopic separation  $\varepsilon^k$  is calculated based on the relative  
257 humidity of soil surface ( $h_a$ ) and soil pore ( $h_s$ ).

$$\varepsilon^k = (h_s - h_a) * \left(1 - \frac{D_l}{D}\right) * n \quad (29)$$

258 Where  $D_l$  and  $D$  denote the diffusivities of water vapor molecules containing heavier isotope and the  
259 lighter isotope, respectively. The ratio can be acquired in Horita et al., (2008) for  $^2\text{H}$  (0.9877) and  $^{18}\text{O}$   
260 (0.9859).  $n$  is an advection term ranging between 0.5 (in saturated soils) and 1 (in dry soils). The factor  
261 is included in calibration for the fractionation of top soil evaporation yet fixed as 0.5 for that of channel  
262 evaporation.

263

### 264 **2.2.3 Water age and travel time**

265 EcoTWIN can track the age of water i.e., the time since water enters the catchment as precipitation,  
266 in each storage. In age tracking, precipitation is defined as new water with age of zero. At the end of  
267 each time step, water ages of all storages are advanced based on the temporal resolution (for instance  
268 one day if the model is set up for daily timesteps). Note that in some circumstances, the modellers  
269 might need to disable the age evolution of specific storage(s) (e.g., groundwater storage) as the  
270 storage can be too large to achieve steady states in model spin-up. Similar to isotopes, water ages are  
271 only controlled by hydrological transport with the same mixing strategy (i.e., complete mixing except  
272 for groundwater).

273 The water ages in EcoTWIN are the mean values averaged from all water molecules in the storage,  
274 which might be dominated by the inflow of very old water that obscure the age distribution of the  
275 young water (e.g., the groundwater input to top soils due to the groundwater extraction for irrigation).  
276 Therefore, EcoTWIN additionally provides the estimation of travel time - the time of water molecule  
277 travelling through each storage. The simulation is similar to that of water ages. The only difference is  
278 that the transition of water between storages (e.g., percolation into deeper soil layers) resets the travel  
279 time to zero. Accordingly, all the water enters a new storage becomes new water instead of just  
280 precipitation in water age tracking.

281



### 282 2.3 Nitrogen module

283 The nitrogen module describes the mass balance of nitrogen, particularly nitrate as the main form of  
 284 dissolved nitrogen, which is dominated by the interaction of hydrological transport and  
 285 biogeochemical transformations.

286 For each timestep, the nitrate concentration is simulated in each storage following three processes –  
 287 hydrological transport/mixing, nitrogen inputs, and biogeochemical transformations. Fully integrated  
 288 with hydrological module, nitrate transport also aligns with hydrological fluxes following the same  
 289 mixing strategy as in the isotopic simulation. For nitrogen sources, EcoTWIN considers the inputs from  
 290 fertiliser, manure, and plant residues, whose annual inputs can be specified via configuration. Notably,  
 291 fertilization can be parameterised via spatial raster inputs if corresponding dataset is available. The  
 292 timing and extent of nitrogen addition of all sources are determined following the implementation in  
 293 HYPE (Lindström et al., 2010), which distributes the annual sum across a specified period (e.g., the  
 294 period between planting and harvest for crops). Additionally, wet deposition is conceptualised as the  
 295 atmospheric nitrogen source, whose concentration can be specified via spatial raster and simply as a  
 296 constant value.

297 The biogeochemical transformations are mainly modified from the mHM-Nitrate model (Yang et al.,  
 298 2018), and the HYPE model (Lindström et al., 2010), which are conceptualised for soil profile and  
 299 channel network. In the soil profile, three nitrogen pools are conceptualised for each soil layer,  
 300 including an inactive nitrogen pool ( $SN_i$ ), an active nitrogen pool ( $SN_a$ ), and a dissolved nitrate pool  
 301 ( $DN$ ). The soil transformations include degradation ( $Dgd_s$ , from  $SN_i$  to  $SN_a$ ), mineralisation ( $Minr_s$ ,  
 302 from  $SN_a$  to  $DN$ ), denitrification ( $Deni_s$ , from  $DN$  to gaseous  $N_2$ ), and plant uptake ( $Uptk_s$ ,  $DN$   
 303 removal).

$$Dgd_s = SN_i * ref_{Dgd,s} * f_{Ta} * f_{\theta} / dt \quad (30)$$

$$Minr_s = SN_a * ref_{Minr,s} * f_{Ta} * f_{\theta} / dt \quad (31)$$

$$Deni_s = DN * ref_{Deni,s} * f_{Ta} * f_{\theta,deni} * f_{conc,s} / dt \quad (32)$$

304 where  $ref_{Dgd,s}$ ,  $ref_{Minr,s}$ ,  $ref_{Deni,s}$  are the parameters representing the reference rates of soil  
 305 degradation, mineralisation, and denitrification.  $f_{Ta}$  and  $f_{\theta}$  are the regulating factors of temperature  
 306 and moisture.

$$f_{Ta} = 2^{(T_a - 20)/10} * \omega \quad \text{where } \omega = \begin{cases} 1 & T_a > 5 \\ T_a/5 & 0 \leq T_a \leq 5 \\ 0 & T_a < 0 \end{cases} \quad (33)$$

$$f_{\theta} = \min \left[ \frac{(1 - p_{\theta,deni}) * (\theta_{fc,i} - \theta_i)}{p_{\theta,fc} * d_i}, \frac{(\theta_i - \theta_{wp,i})}{p_{\theta,wp} * d_i} \right] \quad (34)$$

307 where  $p_{\theta,fc}$  and  $p_{\theta,wp}$  are the empirical factors that are fixed as 1.2, 0.8 based on literature values  
 308 (Lindström et al., 2010; Yang et al., 2018).  $p_{\theta,deni}$  is the saturation threshold for soil denitrification  
 309 ranging between 0.4 – 0.85 (Yang et al., 2018). A different moisture factor considering a saturation



310 threshold ( $\theta_{thres}$ ) is employed for denitrification, as denitrification is more sensitive to the soil  
311 wetness condition:

$$f_{\theta,deni} = [(\theta_i/\theta_{fc,i} - \theta_{thres})/(1 - \theta_{thres})]^{2.5} \quad (35)$$

312 The process is additionally controlled by the concentration level in the storage  $f_{conc,s} = C/(C + 10)$ .  
313 Plant uptake is simulated using a three-parameter logistic growth equation in (Eckersten et al., 1994;  
314 Lindström et al., 2010).

315 Currently, in-stream denitrification is the only process considered in EcoTWIN.

$$Deni_w = ref_{Deni,w} * f_{T_w} * f_{conc,w} * A/dt \quad (36)$$

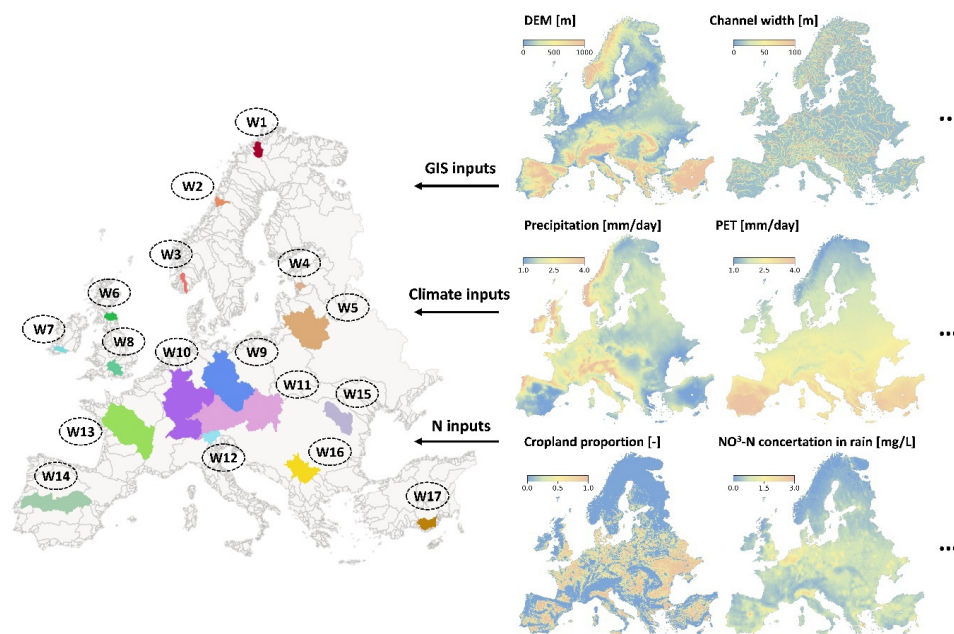
316 where  $ref_{Deni,w}$  is the reference in-stream denitrification rates. The actual rates are regulated by a  
317 concentration factor  $f_{conc,w} = C/(C + 1.5)$  and a temperature factor  $f_{T_w}$  (the same equation for  $f_{T_a}$   
318 with inputs substituted by river temperature  $f_{T_w}$ , simplified as the rolling-average of 20-day air  
319 temperature).

320

### 321 **3 Model calibration and validation**

322 To examine the capacity of EcoTWIN to reproduce ecosystem functioning, the model is tested and  
323 validated via two aspects – (i) the ability to reproduce the calibrated observations and (ii) to capture  
324 the general spatio-temporal patterns of internal fluxes with important ecohydrological implications  
325 yet not included in calibration (e.g., evapotranspiration). To ensure model generality, 17 catchments  
326 are selected for calibration and validation, which span a wide range of characteristics in geography,  
327 climate, and anthropogenic managements (Figure 2 and Table 1). Anthropogenic management  
328 practices have a less dramatic effect than climate and geography in most catchments due to the  
329 relatively low proportion of urbanized areas. However, a few notable exceptions—such as the Rhine,  
330 Elbe, and Danube catchments—are included in the analysis, as these densely populated regions hold  
331 critical ecological, agricultural, and economic importance for Europe, and are subject to intensive  
332 human interventions in water management. This also provides a chance to examine the applicability  
333 of EcoTWIN in human-affected catchments.

334



335

336 Figure 2. The selected catchments for model validation and an overview of inputs.

337

338 Table 1. Characteristics of the selected catchments. **Lat** depicts the latitude of upper left corner of the  
 339 catchment. **DEM** and **Area** are the mean elevation in m.a.s.l. and catchment size in km<sup>2</sup>. **Precip**, **Temp**,  
 340 and **PET** are the annual averages of precipitation, air temperature, and potential evapotranspiration  
 341 in mm/yr.  $f_{crop}$ ,  $f_{forest}$ , and  $f_{urban}$  are the fractions of cropland, forest, and urbanized areas in 2019  
 342 in %. Null means no name is assigned for the catchment in the Catchment Characterisation and  
 343 Modelling (CCM) database.

ID	Name	Lat	Area	DEM	Precip	Temp	PET	$f_{crop}$	$f_{forest}$	$f_{urban}$
1	Null	70.0	8725	468.5	448.5	-1.8	442.8	<1	1.9	<1
2	Vefsna	65.9	5475	636.5	1260.8	0.7	433.6	<1	24.6	<1
3	Null	59.8	5225	742.3	1400.9	3.0	545.7	<1	39.8	<1
4	Null	58.3	4350	67.4	654.5	6.4	667.9	17.4	60.5	1.4
5	Nemunas	56.6	97550	147.9	599.3	7.1	730.6	33.0	39.1	4.5
6	Tweed	55.9	6250	264.3	1023.4	7.9	600.9	21.8	18.9	1.4
7	Null	52.3	4300	175.4	1218.1	10.1	645.2	12.1	17.4	1.9
8	Thames	52.2	11900	112.0	700.7	10.4	782.9	44.9	14.1	22.0
9	Elbe	53.5	130225	318.3	626.9	8.8	836.3	41.2	34.6	10.8
10	Rhine	52.0	170175	508.3	943.3	8.9	821.0	21.5	41.2	17.1
11	Danube <sub>(a)</sub>	50.5	197600	618.0	843.6	8.3	857.4	28.5	37.1	11.5
12	Adige	47.2	11600	1771.9	1002.3	4.5	809.7	<1	48.8	3.2
13	Loire	48.7	122125	298.9	778.7	11.0	887.4	37.6	25.7	6.5
14	Tajo	40.4	75575	686.2	549.5	14.3	1359.6	26.7	34.5	3.3
15	Danube <sub>(b)</sub>	48.4	37975	533.3	534.7	8.1	869.5	32.0	41.3	6.4
16	Danube <sub>(c)</sub>	44.8	37725	653.3	684.7	9.7	994.2	12.8	44.3	5.8



344 17          Null    37.6    12650    1384.5    454.1    12.2    1256.9    5.9    4.3    <1

345 **3.1 Model setup and calibration**

346 EcoTWIN was setup for each of the 17 catchments for calibration with a spatial resolution of 5 km<sup>2</sup>  
 347 and a temporal resolution of daily timesteps from 1980 to 2024. As a fully distributed model, gridded  
 348 GIS inputs are used in the model setup, including a digital elevation model, flow direction, slope,  
 349 channel width, channel length, proportion of each land use type (Winkler et al., 2021), proportions of  
 350 each soil type (world soil map, WRB2014), and soil properties (e.g., depth-dependent proportions of  
 351 clay, sand, silt, and organic matter from SOILGRIDS). All spatial inputs were acquired with finer  
 352 resolution (50 m or above) and resampled to the resolution of this application (5 km).

353 The climatic variables used to drive EcoTWIN include precipitation, air temperature, potential  
 354 evapotranspiration, relative humidity, and a few variables that are optional required for the  
 355 calculation of channel evaporation (air pressure, net radiation, and wind speed). These climatic  
 356 variables are available from the reanalysis products ERA5 and E-OBS, while PET is calculated using FAO  
 357 Penman-Monteith equation. For nitrogen simulations, additional inputs are needed including the  
 358 fertilization map (Grizzetti et al., 2021) and nitrate concentration of rainfall (Zhu et al., 2025) as the  
 359 boundary of nitrogen addition from agricultural activities and wet deposition.

360 The calibration was conducted separately for each catchment to test the applicability of EcoTWIN  
 361 under different geological and climatic contexts. Three commonly used variables for hydrological and  
 362 water quality modelling (discharge, stream water isotope composition, and in-stream NO<sub>3</sub>-N  
 363 concentrations) are employed for calibration. Their long-term time series were acquired at daily steps  
 364 from different sources (discharge from GRDC, isotopes from Wateriso and GNIR, and NO<sub>3</sub>-N  
 365 concentration from global water quality database, GEMStat), and then compared with simulation  
 366 results at multiple sites for each catchment. Here <sup>18</sup>O was selected for isotopic validation due to its  
 367 higher precision and data abundance. Given the discrepancy in duration of observations (especially  
 368 for isotopes and NO<sub>3</sub>-N), a separate calibration and validation based on a split-sample approach is  
 369 difficult. Therefore, the full timescale (1982 - 2024) was used for calibration (and the validation  
 370 introduced in Section 3.2).

371 The DiffeREntial Evolution Adaptive Metropolis algorithm (DREAM) was selected for parameter  
 372 optimisation due to its relatively efficient and effective performance for high-dimensional problems  
 373 (as benchmarked in Wu et al., 2025c). The algorithm was implemented separately for each catchment  
 374 with the same prior distribution of parameters (Table S1). The maximum iteration was set as 100,000  
 375 for each catchment (20 chains with maximum chain length of 5000), from which 40 best simulations  
 376 were selected from the posterior distribution. The Kling-Gupta efficiency (KGE) statistic was used to  
 377 construct an informal likelihood function for DREAM optimisation.

378 
$$l = \left[ \sum_{i=1}^{N_{obs}} \sum_{j=1}^{N_{site}} (1 - KGE) * w_{i,j} \right]^{-m}$$



379 Where  $N_{obs}$  and  $N_{site}$  are the number of observation types (3) and sites. The weight  $w_{i,j}$ , defined for  
380 observation type  $i$  at site  $j$ , is assigned equally across sites such that the total weight for each  
381 observation type sums to  $1/3$ .  $m$  is an exponentially coefficient to stretch the likelihood surface that  
382 is often set based on the number of observation points. After prior test run,  $m$  was set as 500. Finally,  
383 the likelihood function is transformed to logarithmic form for numeric stability.

384

### 385 **3.2 Model validation**

386 Reanalysis products were further employed to validate uncalibrated internal model states or fluxes  
387 from three important perspectives in ecohydrological modelling – snow depth from ERA5,  
388 evapotranspiration from MODIS, and surface water mass anomaly from GRACE (as a storage proxy).  
389 The simulated variables corresponding to these products are, respectively, the depth of snow pack,  
390 the sum of soil evaporation, channel evaporation, and transpiration from all soil layers, and the  
391 anomaly of total water storage above groundwater (i.e., the sum of canopy storage, snow, soil water  
392 storages, and vadose storage). The validation was realised via resampling the remote sensing products  
393 to 5 km and comparing grid-to-grid with the modelled outputs. Note that  $r^2$  was used as the  
394 performance metrics, as KGE is not applicable for time series with zero average, yet the average of  
395 surface mass anomaly is close to 0.

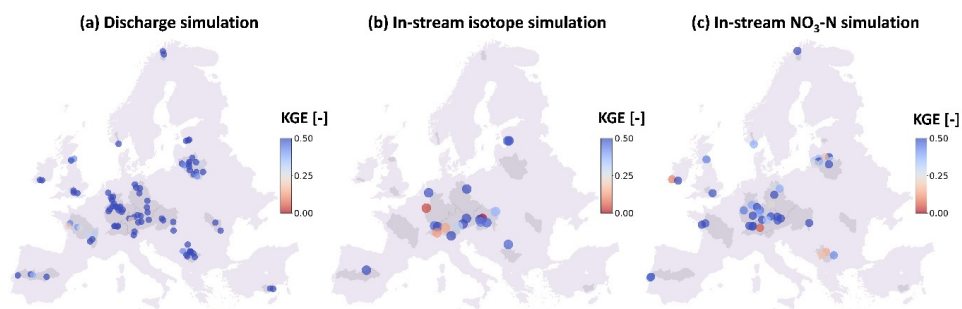
396

## 397 **4 Results**

### 398 **4.1 Simulation performance**

399 Generally, EcoTWIN successfully reproduced the observed discharge in all 17 catchments with KGE  
400 exceeding 0.5 at most site (Figure 3a). This is further demonstrated in Figure 4 where both seasonality  
401 and peaks of discharge with different levels of magnitudes were captured. Similarly, isotopic and  
402 nitrate simulations also produced good performances at most sites (Figure 3b). However, there are a  
403 few exceptions. The failure of isotopic simulations was found at two sites within the Alpine region  
404 (bottom left corner of figure 3b). This can be attributed to the uncertainty in precipitation and  
405 snowmelt isotopes (Ala-aho et al., 2017), the incorrect isotopic composition in groundwater, or the  
406 reduced applicability of degree-day model for mountainous areas in Europe. Nitrate simulations also  
407 failed to capture the observations at three sites. However, as is shown in Figure 4, these sites have  
408 relatively low levels of  $\text{NO}_3\text{-N}$  concentrations. Such low average values can easily trigger the  
409 degradation of the KGE statistic as one of the sub-components is highly sensitive to the mean deviation,  
410 though the absolute deviation remained low (Figure 4). Given the good performance at the remaining  
411 sites, we concluded that EcoTWIN has the capacity to reproduce in-stream components for a wide  
412 range of catchments and for relatively long periods.

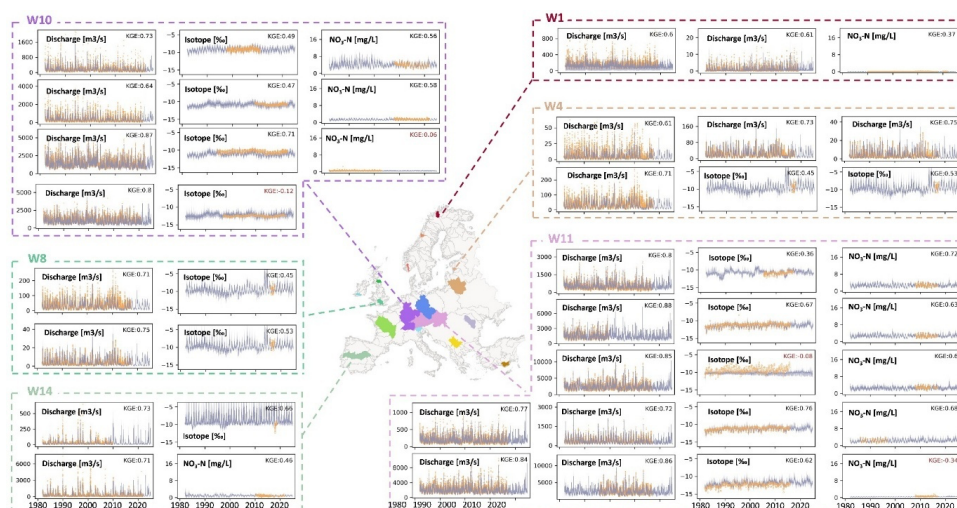
413



414

415 Figure 3. The simulation performance of discharge, in-stream isotope, and in-stream NO<sub>3</sub>-N.

416



417

418 Figure 4. The simulated (blue) and observed (orange) time series of discharge, isotopes, and NO<sub>3</sub>-N at  
419 representative gauges. Note that the sites with relatively poor performance (KGE < 0.2) were  
420 particularly shown for model diagnosis.

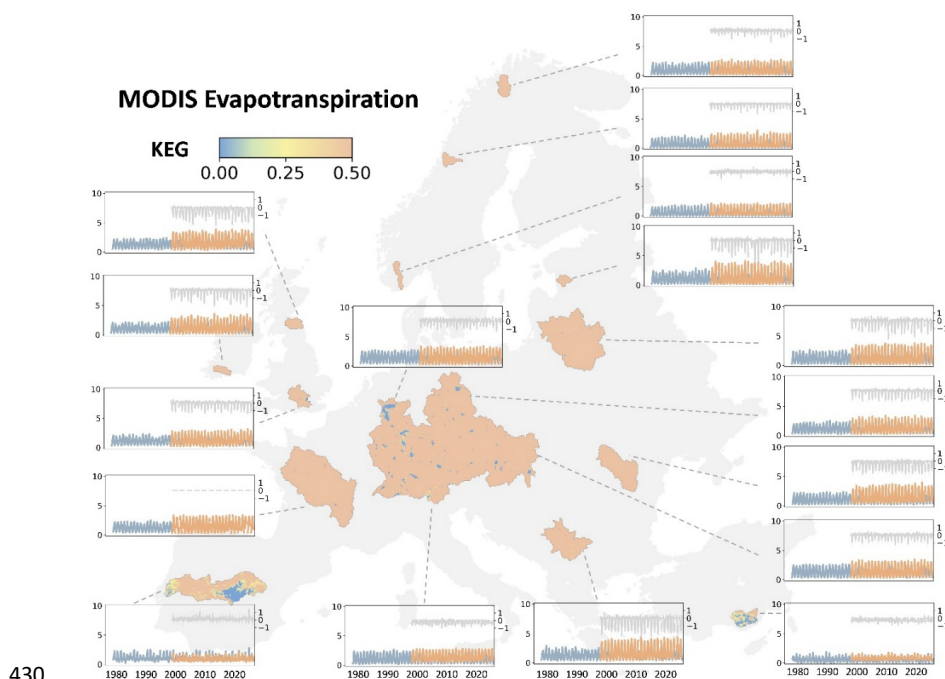


421

## 422 4.2 Validation

423 Apart from the variables used for calibration, three internal states and fluxes are also compared with  
424 remote sensing products. First, the sum of soil evaporation, channel evaporation, and transpiration  
425 was compared to MODIS evapotranspiration in each grid cell. The results in Figure 5 shows a general  
426 good fit between simulation and observation with  $r^2$  above 0.5 in most regions. From the subplots in  
427 Figure 5, we can see that the seasonality and magnitude of evapotranspiration were well captured  
428 though the peaks in summer were slightly underestimated.

429



430

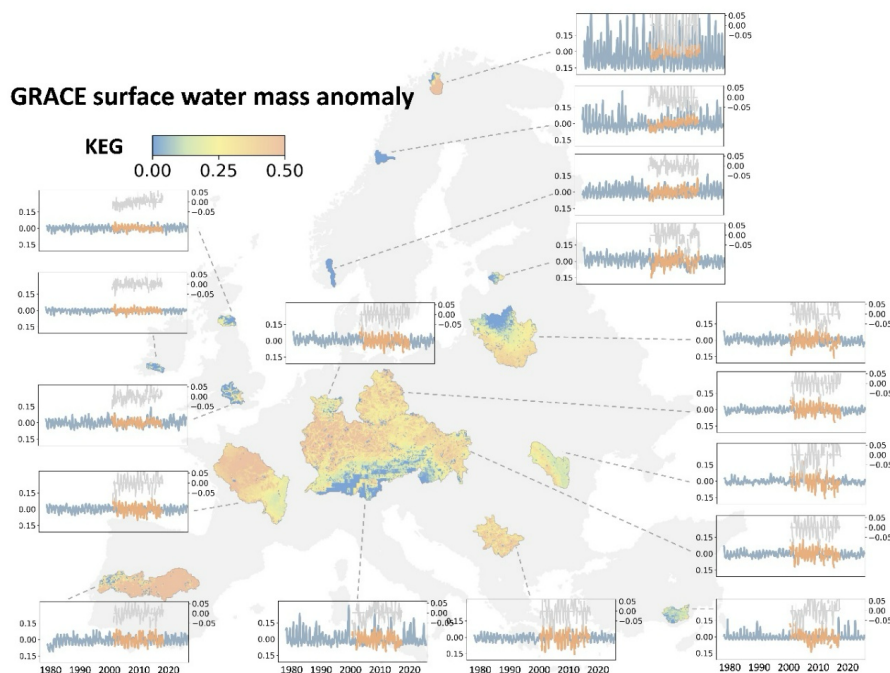
431 Figure 5. The grid-to-grid comparison between simulated evapotranspiration and MODIS  
432 evapotranspiration. The time series show the monthly mean of simulated (blue) and observed (orange)  
433 values, as well as the deviations (grey).

434

435 Then, the water storage anomaly was compared to the anomaly of simulated surface storage, i.e., the  
436 sum of canopy storage, snow, soil water storages, and vadose storage. The grid-to-grid comparison in  
437 Figure 6 shows a general good fit in most regions with  $r^2$  close to or above 0.5. However, more  
438 degradation was found compared to the performance in evapotranspiration, especially in coastal  
439 regions. For instance, GRACE exhibited considerably increasing trends in water storage between 2005  
440 to 2015 in two Nordic catchments (W2 and W3), yet our simulations only showed a moderate

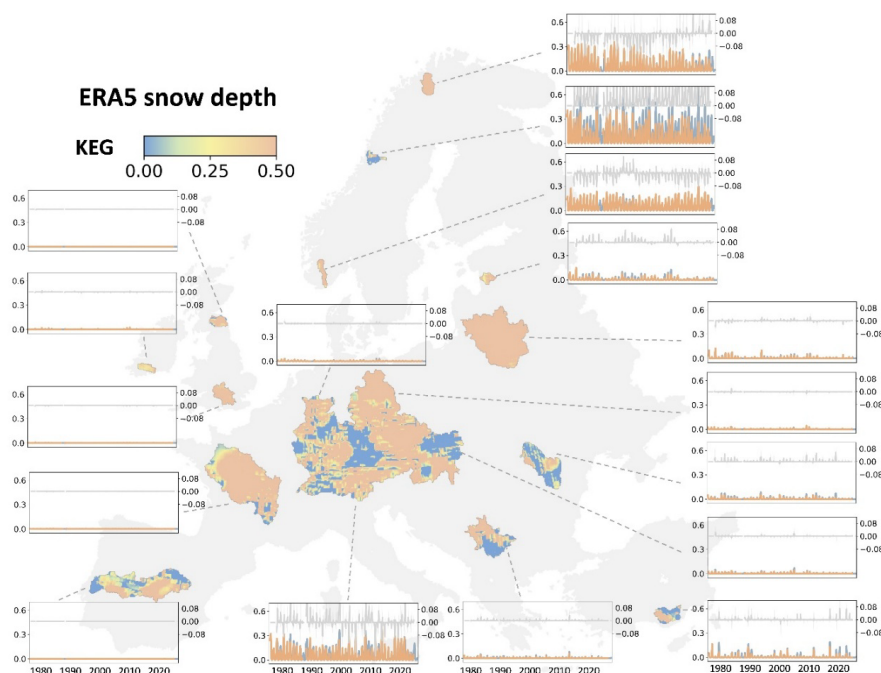


441 increasing trend. Similar degraded performance was found in the coastal catchments (e.g., three  
442 British catchments W6-8 in UK), though the magnitudes of simulation and observations fit well. This  
443 is possibly attributed to the coarse resolution of GRACE which additionally considered the storage mass  
444 from ocean in coastal region yet not included in this terrestrial-explicit modelling.



445  
446 Figure 6. The grid-to-grid comparison between simulated water storage anomaly and GRACE surface  
447 water mass anomaly. The time series show the monthly mean of simulated (blue) and observed  
448 (orange) values, as well as the deviations (grey).

449  
450 Finally, the simulated snow depth was compared to the ERA5 reanalysis products. Results in Figure 7  
451 show a good agreement between simulations and observations in most regions with  $r^2 > 0.5$ , though  
452 degradation was found in a few catchments. Note that, the poor performances were generally found  
453 in catchments with limited snow accumulation, e.g., W14-17 in subplots in Figure 7. In the other words,  
454 the absolute deviation was relatively limited for snow depth simulation.



455

456 Figure 7. The grid-to-grid comparison between simulated snow depth and ERA5 snow depth. The time  
457 series show the monthly mean of simulated (blue) and observed (orange) values, as well as the  
458 deviations (grey).

459

#### 460 4.3 Simulated water age and its link to water quality

461 Like many existing distributed hydrological and water quality models (e.g., SWAT, mHM, Ech<sub>2</sub>O-iso,  
462 HYPE etc.), EcoTWIN can provide estimation of main ecohydrological fluxes at high spatial and  
463 temporal resolutions, including canopy interception, snow melt-accumulation, infiltration, percolation  
464 through soil layers, groundwater recharge, and lateral flux routing at different horizontal phrases.  
465 Among these variables, a unique trait of EcoTWIN lies in its capacity to track water fluxes via isotopes,  
466 thus being able to provide a consistent estimate of water age and travel times. Therefore, in Figure 8,  
467 both variables are shown as the long-term average from 1982 to 2024 for soil profile and stream water.

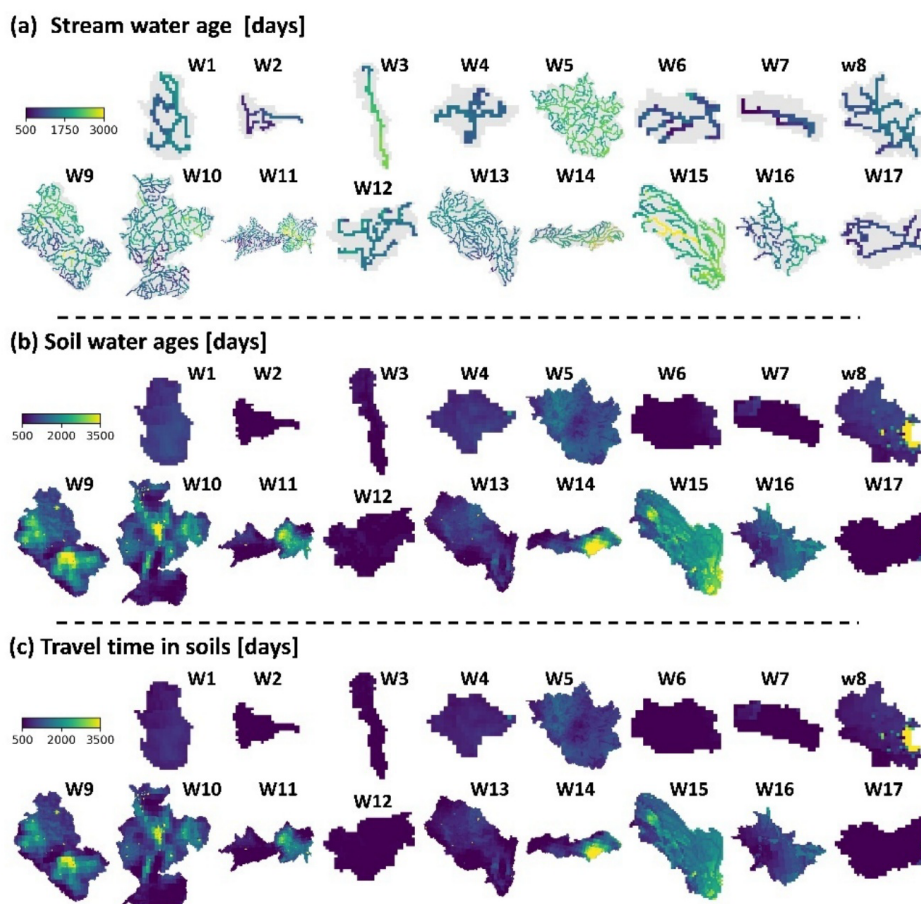
468 Generally, the magnitudes of water ages follow the geographic and climatic gradients, with younger  
469 water found in catchments with higher annual precipitation inputs. Those regions locate in the north-  
470 west coast of Europe (Figure 2), particularly for Nordic catchments where lower temperature and net  
471 radiation further limit the level of potential evapotranspiration, leading to larger percolation to deeper  
472 soil layers and groundwater. Such high turnover rates of water in these catchments (W1, W2, W3, W4,  
473 W5, and W8) are also demonstrated as the simulated travel time in soil profile with average values  
474 remaining below 500 days.



475 A similar pattern was also found in mountainous regions with higher precipitation and lower potential  
476 evapotranspiration compared to lowland areas. Two clear examples are W12 and W17 located in the  
477 Alps and the Taurus Mountains where water ages and travel time remained below 500 days (Figure  
478 2). In specific wet periods, the water ages and travel time can be reduced to just days, suggesting the  
479 rapid response of saturated hydrological systems (e.g., the wet year 1999 in Europe in Figure S1-S3).  
480 In contrast, the lowlands in central-west Europe showed much slower turnover rates, with the mean  
481 water ages reaching almost 10 years in some specific regions. A few examples could be found in the  
482 three major representative catchments in Central Europe – Elbe, Rhine, and Danube (W9-11). Such  
483 old water ages and long travel time are further exacerbated during dry years (e.g., 2004, a drought  
484 year for much of Europe shown in Figure S1-3).

485 Note that though water ages and travel time share similar magnitudes and spatial patterns. It is partly  
486 attributed to the fact that the travel time in the conceptualised storages increases exponentially in a  
487 sequential order. Taking the Rhine as an example, the average travel time in top soil layer, median soil  
488 layer, deep soil layer are 65, 225, 1291 days, respectively. Such a depth-dependence profile makes the  
489 overall ages/travel time follow the magnitude of bottom layer and leads to similarity between water  
490 ages and travel time. However, large discrepancies are possible between the two indices if a shallow  
491 lower boundary is adopted.

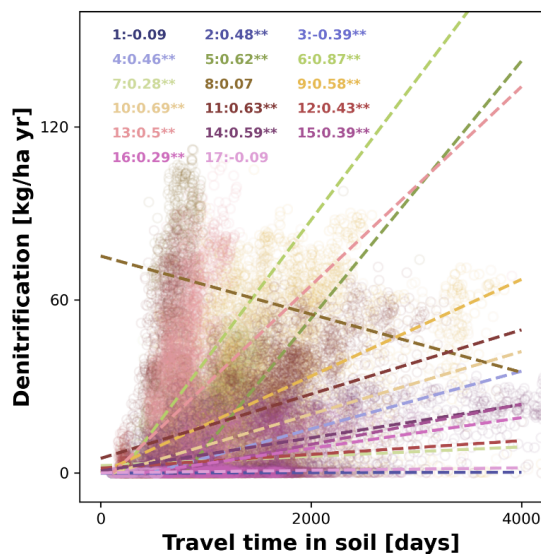
492



493

494 Figure 8. The simulated long-term average (1982-2024) of water age and travel time in channel and  
495 soil profile. Water ages represent the time since water enters the catchments as precipitation, while  
496 travel times depict the residence time of water within the specific storage.

497



498

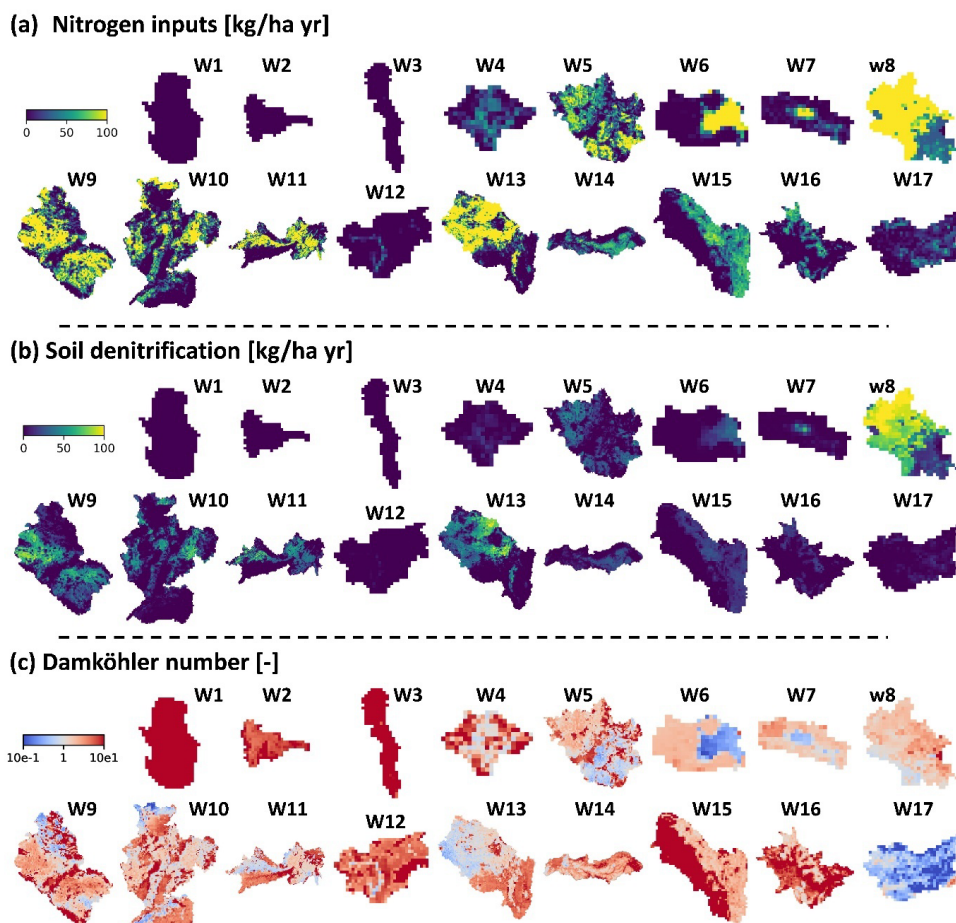
499 Figure 9. The correlations between travel time and annual denitrification. The text depicts the  
500 spearman correlation coefficients and p values (\* = less than 0.05, \*\* = less than 0.01) in each  
501 catchment.

502

503 The estimation of travel time and water ages further provides opportunities to link hydrology and  
504 water quality processes in the modelling framework. The simplest and most intuitive way is to  
505 compare travel times and simulated biogeochemical process kinetics. Taking denitrification as an  
506 example, we applied linear regression and Spearman's correlation test to investigate the potential  
507 correlation between travel time of soil water and denitrification rates. The results in Figure 9 showed  
508 the strong positive correlations in most agricultural-dominated catchments (W5, W5, W6, W8, W9,  
509 W11) yet only weak or no correlation in remaining pristine watersheds. This suggests that travel time  
510 might be a key control on soil nitrogen removal in European croplands.

511 More insights can be gained via examination of the Damköhler Number, which quantifies the ratio  
512 between timescales of chemical transport and transformation. Here in our modelling framework, it  
513 can be calculated as the ratio between the travel time of soil water and the time for all soil NO<sub>3</sub>-N  
514 storage to be removed under the simulated denitrification rates. As shown in Figure 10c, the long-  
515 term averages of Damköhler number remain below 1 in most croplands, supporting the conclusion  
516 from the linear regression (travel time is a major limiting factor on soil nitrogen removal). Via the  
517 spatial- and temporal-explicit estimation of Damköhler number, EcoTWIN provides the opportunity to  
518 bridge the catchment hydrological and water quality with travel time.

519



520

521 Figure 10. The simulated long-term average (1982-2024) of nitrogen inputs, soil denitrification, and  
522 Damköhler number.

523

## 524 **5 Discussion**

### 525 **5.1 Structural and Functional Merits of EcoTWIN**

526 As a new tracer-aided ecohydrological model, EcoTWIN has a novel advantages compared to previous  
527 models. In this section, we briefly introduced the merits in model structure, applicability, and insights  
528 from tracer-aided simulation.

#### 529 **5.1.1 Integrated C++ framework**

530 Applications of large-scale modelling have been increasingly popular due to the accelerating  
531 development of observation networks and availability of remote sensed data. However, it increases  
532 severely increases the computational burden of ecohydrological modelling. Especially for fully



533 distributed models, increasing size of the model domain can lead to exponential increase in  
534 computation demands. In this context, an integrated C++ framework can significantly accelerate the  
535 modelling tasks, as all computation can be conducted within memory thereby avoiding the additional  
536 input/output overhead associated with disk-based operations in loosely coupled model chains (e.g.,  
537  $\text{Ech}_2\text{O}$ -iso-nitrate; Yang et al., 2024). A standard test was not performed, but based on our modelling  
538 experience in the same catchment with different models, the speed of EcoTWIN (~5 seconds for a  
539 simulation with 285 grid cells and 30 years at daily timestep) is close to the water quality model mHM-  
540 Nitrate (~5 seconds yet without isotopic simulations; Wu et al., 2022) and easily outperforms  $\text{Ech}_2\text{O}$ -  
541 iso-nitrate (7 minutes; Wu et al., 2025b).

#### 542 **5.1.2 Selective disassembly structure**

543 EcoTWIN incorporates a wide range of ecohydrological processes from canopy to groundwater, which  
544 not only include natural processes but also anthropogenic activities like irrigation. Land managements  
545 can also be represented by dynamical parametrisation, thus enabling EcoTWIN to function as a  
546 learning tool to investigate the impacts of changes in anthropogenic management over natural  
547 ecosystems; for instance, the land use distribution was updated every 10 years in our test examples  
548 to reflect the moderate increases in afforestation in the past 45 years in Europe. More importantly,  
549 unlike hard coded process representations/equations in most ecohydrological models, EcoTWIN has  
550 a selective disassembly structure, which provides alternative conceptualisations for several important  
551 hydrological processes (canopy interception, percolation, groundwater recharge, as well as three  
552 pedotransfer functions for initialising soil properties). Modellers can benefit from such flexible model  
553 structure by either selecting process representations best suited to field knowledge or data prior to  
554 calibration, or integrating module selection into the calibration thus enabling simultaneous  
555 optimisation of model structure and corresponding parameters. The latter aspect, i.e., the  
556 optimisation of model structure, can be realised together with the recently developed optimisation  
557 algorithm DREAM<sub>(LOAX)</sub> that aims to identify the deficits in model structure during calibration (Wu et  
558 al., 2025a).

#### 559 **5.1.3 Transferability to contrasting geographic and climatic contexts**

560 To thoroughly test the applicability of EcoTWIN, 17 catchments with different climatic and  
561 geographical contexts were selected for validation, spanning over most biomes in Europe, from snow-  
562 dominated watersheds in Nordic or alpine regions, to agricultural-influenced lowlands catchments,  
563 and Mediterranean ecosystems (Figure 1 and Table 1). Through multi-criteria calibration against three  
564 objectives at multiple sites, the model successfully reproduced the seasonality and peaks of discharge,  
565 in-stream isotopes, and  $\text{NO}_3\text{-N}$  concentrations in most catchments. Such performance is comparable  
566 or better than the previous model benchmarks at similar scales (Bajracharya et al., 2023; Mikayilov et  
567 al., 2015; Rakovec et al., 2016, 2019). Note that the concentration of  $\text{NO}_3\text{-N}$  was used for calibration,  
568 whose accurate simulation is more difficult than  $\text{NO}_3\text{-N}$  loads given the naturally good performance in  
569 discharge. In the other words, hydrological simulation is often the least problematic part in integrated  
570 water quality modelling, as it is mostly dominated by natural catchment properties while nitrogen



571 cycling is more interfered by anthropogenic managements (e.g., fertilization and irrigation) (Wu et al.,  
572 2025b). Additionally, the simulated internal fluxes were also compared to three reanalysis products in  
573 hydrological simulations, corresponding to the key fluxes or storage states in hydrological cycling  
574 (snow melt-accumulation, evapotranspiration, and water storage). The results show that constrained  
575 by isotopes, EcoTWIN was able to reproduce comparable hydrological modelling results to the remote  
576 sensing observations without direct calibration regarding magnitudes, spatial patterns, and temporal  
577 dynamics. The only degraded performance was found in GRACE surface mass anomaly in coastal  
578 regions. There are two potential reasons: (i) the coarse resolution of GRACE might account for mass  
579 shifts in both ocean and land, yet EcoTWIN only produces mass anomaly in terrestrial systems; (ii)  
580 bidirectional fluxes across the land-ocean interface might drive key changes in coastal systems, which  
581 is not considered in current version of EcoTWIN. Nonetheless, given the relatively good agreement  
582 with most available observations, we conclude that EcoTWIN is applicable across a range of terrestrial  
583 ecosystems from boreal to temperate and subtropical climate.

#### 584 ***5.1.4 Bridging hydrology and water quality with water ages***

585 Further to the inference of hydrological and nitrogen processes that is also available in other  
586 distributed water quality models (Wellen et al., 2015), one unique trait of EcoTWIN lies in its capacity  
587 to track water fluxes and ages with stable water isotopes. As a tracer-aided model, EcoTWIN not only  
588 simulates the celerity of catchment response, but tracks the velocity of water via different flow paths.  
589 The importance of delineating flow paths within catchments has long been recognized by hydrologists,  
590 and has motivated the development of many indices to describe the movement of water molecule at  
591 catchment-scale and estimate associated timescales (Sprenger et al., 2019). A few examples are water  
592 ages, transient time distribution, and young water fractions (Benettin et al., 2015; Hrachowitz et al.,  
593 2013; Jasechko et al., 2016). However, those indices are mainly calculated in a lumped manner where  
594 different flow paths in the catchment are characterised as a black box, thus characterising the overall  
595 input-output dynamics yet potentially omitting important spatio-temporal variability of hydrological  
596 boundary conditions. Instead, EcoTWIN, benefiting from the gridded-based structure, can utilise the  
597 increasingly available spatial information (e.g., gridded remote sensing datasets) thus characterising  
598 the water ages and travel time in a spatially-explicit manner. Note that simulations of water age/travel  
599 time, like other ecohydrological processes, are sensitive to spatial resolution. The coarse resolution  
600 used for large catchments (e.g., 5 km in this study) may obscure the sub-grid heterogeneity. For  
601 instance, local hydrological hotspots characterized by short travel times and young water ages can be  
602 damped or averaged out at coarser resolutions, as reported in modelling studies using ECH2O-iso  
603 (Smith et al., 2021; Yang et al., 2023b). However, this limitation can be mitigated by increasing spatial  
604 resolution, and it does not undermine the utility of EcoTWIN for water-tracking.

605 Compared to water age which quantifies age of water within the system, travel time, accounting for  
606 the water age within a specific storage, is more important in understanding the links between  
607 hydrological and nutrient cycles. Such index, also known as transient time or exposure time, forms  
608 one of the bases for water quality modelling. Therefore, the travel time estimated by EcoTWIN has  
609 potential to improve the simulation of biogeochemical transformations in water quality models with



610 simplified hydrological modules (e.g., MONERIS; Bonchkovsky & Osadcha, 2024). Moreover, travel  
611 time can be used as a proxy to bridge hydrological processes and biogeochemical transformations.  
612 Here we presented a simple framework to calculate the Damköhler Number for denitrification. By  
613 using the simulated travel time and reaction timescale (i.e., the time for full removal of nitrogen  
614 storage under current denitrification rates), estimation of Damköhler Number was achieved in a  
615 spatially- and temporally-explicit manner (Figure 9), which can highlight where and when soil nitrogen  
616 removal is constrained by the limited exposure time in the catchment. Such high-resolution  
617 information is unique, as the use of this index has been largely restricted to steady-state groundwater  
618 systems or riparian/hyporheic zones due to the difficulty in quantifying processing time and residence  
619 time at larger scales (Ocampo et al., 2006; Wu et al., 2022).

620

## 621 **5.2 Limitations and roadmap for future development**

622 Despite these unique traits, EcoTWIN has limitations. In this section, the uncertainties in model  
623 structure and conceptualisation are introduced, as well as the potential roadmaps for future  
624 developments.

### 625 **5.2.1 Potential towards physics-based conceptualisation of groundwater**

626 Groundwater in EcoTWIN is characterised as a single-layer storage linking with adjacent upstream and  
627 downstream storages following the topographic gradients. Such conceptualisation, although it has  
628 been widely employed in hydrological models (e.g., SWAT, mHM, EcH<sub>2</sub>O, STARR, etc.), does not align  
629 with the physical mechanisms of groundwater routing, as groundwater flow direction follows the  
630 hydraulic gradients which may not entirely coincide with topographic gradients (Condon et al., 2021).  
631 Such simplified routing has less effect in large catchments with clear topographic gradients (e.g., Rhine  
632 starting from Alps to North plain), yet might cause biased estimation in water mass balance for flatter  
633 headwater catchments (Yang et al., 2025). Therefore, we plan to further incorporate an additional  
634 groundwater module to realise physics-based routing following the Darcy's Law in future.

### 635 **5.2.2 Revisiting mixing strategies**

636 Mixing strategy is a key component in water quality or tracer models describing the flux-storage  
637 behaviours along specific flow paths. There has long been a debate on different mixing assumptions  
638 and theories. A typical example is the two-water-world hypothesis, where water storage in the soil  
639 profile is differentiated into a tightly-bound pool and a mobile-water pool (McDonnell, 2014). Such  
640 conceptualisation is close to the definition of soil matrix flow and preferential flow: the existence of  
641 free-flowing preferential flow will bypass the soil matrix vertically and accelerate the lateral drainage  
642 via direct connection with channel network (Hrachowitz et al., 2013; Sprenger et al., 2019). However,  
643 a complete mixing strategy is often regarded as a reasonable approximation and used in most water  
644 quality and tracer models (Jung et al., 2025). This is not only attributed to its computational simplicity,  
645 but also the difficulty to conceptualise preferential flow in an evidenced-based manner. In the other  
646 words, even with the recognition of preferential flow, its calculation is often hindered by the



647 subsurface heterogeneity in soils and bedrock; a good visualisation is given in Figure 7 in Sprenger et  
648 al., (2019). Alternatively, partial mixing has been developed for ecohydrological models (e.g.,  
649 Hrachowitz et al., 2013), which could be added as a complementary mixing strategy in EcoTWIN.  
650 However, as benchmarked in Hrachowitz et al., (2013), the partial mixing brings only moderate  
651 improvements in simulations yet introduces challenges to model spin-up (the increasing instability of  
652 storage ages due to the exchange between bypass and storage compartment). Moreover, the  
653 realisation of partial mixing, like preferential flow, relies on additional parameters to describe the  
654 timing and extent of mixing thus introducing additional parametric uncertainty. Therefore, we  
655 recommend a rigorous evolution on necessity of partial mixing before any application.

### 656 **5.2.3 Complementing the in-stream biogeochemical processes**

657 Transformation is as crucial as transport in inland-water nitrogen cycling (Wang et al., 2024). In the  
658 current version of EcoTWIN, denitrification is the only in-stream process of nitrogen retention.  
659 However, recent studies have shown that other processes are involved which may be important for  
660 aquatic nitrogen cycling. An example originates from Wang et al., (2024), where global inland-water  
661 modelling shows that in-stream denitrification only accounts for a minor fraction of  $\text{NO}_3\text{-N}$  removal  
662 compared to biological uptake. Though their modelling considers lake and reservoirs where primary  
663 production of benthic plants and algae is usually greater than that in rivers, the in-stream assimilation  
664 might still play a significant role in slow-flowing river systems. This is supported by a recent modelling  
665 study that estimated nitrogen retention at 15-min interval based on high-frequency  $\text{NO}_3\text{-N}$  data (Yang  
666 et al., 2023a). Therefore, we plan to further compliment EcoTWIN with in-stream assimilation  
667 conceptualisation, as well as other potentially important riverine processes (e.g., nitrogen burial in  
668 sediments; Akbarzadeh et al., 2019).

### 669 **5.2.4 Integrated calibration framework to embrace equifinality**

670 Strictly speaking, equifinality is not specifically linked to EcoTWIN, but remains a universal problem for  
671 calibration or parameter tuning for almost all ecohydrological models. It is reflected in multiple  
672 parameters sets yielding similarly good model performance, thus increasing the uncertainty in process  
673 inference. The extent of equifinality is primarily controlled by the magnitude of parameters and  
674 observation/objectives (Wu et al., 2025c). Unfortunately, conceptualisations across diverse process  
675 domains (e.g. for hydrology, isotopes and N-cycling) in EcoTWIN also lead to a relatively large number  
676 of parameters. Such risk in equifinality can be potentially constrained via sensitivity analysis, but can  
677 still remain an issue given the ubiquitous epistemic uncertainty in data and model structure (Beven,  
678 2006, 2015). Alternatively, the recently developed calibration algorithm  $\text{DREAM}_{(\text{LoAX})}$  provides an  
679 opportunity to embrace equifinality by tuning parameters based on the limits-of-acceptability theory  
680 under the equifinality thesis (Wu et al., 2025a). The integrated modelling framework of EcoTWIN and  
681  $\text{DREAM}_{(\text{LoAX})}$  can potentially increase the robustness of model calibration and inference.

682



## 683 **6 Conclusions**

684 Uncertainty is a central concern in ecohydrological modelling, as models are not only used for  
685 prediction of specific variables, but also for process inference (backtracking internal processes from  
686 available observations) that are inherently embedded within considerable uncertainty. Stable water  
687 isotopes can help effectively constrain hydrological fluxes due to their conservative nature, motivating  
688 the increased development of tracer-aided models. However, few attempts have been made to  
689 incorporate a tracer-aided hydrological framework into water quality models.

690 Therefore, we introduce EcoTWIN, a fully distributed tracer-aided *ecohydrological* model that *tracks*  
691 *water*, *isotopic*, and *nutrient* fluxes simultaneously in an integrated C++ framework. To thoroughly  
692 validate the model, 17 large European catchments were selected with a wide range of geographic and  
693 climatic gradients (from snow-dominated watersheds in Nordic or alpine regions, to agricultural-  
694 influenced lowlands catchments, and mediterranean ecosystems). The model was calibrated against  
695 long-term observations of discharge, in-stream isotopes, and NO<sub>3</sub>-N concentrations during 1980-2024  
696 in each of the 17 catchments. Additionally, uncalibrated internal states and fluxes were also compared  
697 with three remote sensing products (ERA5 snow depth, MODIS evapotranspiration, and GRACE  
698 surface water anomaly) to validate the credibility of process inference.

699 The generally good agreements in both calibrated in-stream components and uncalibrated internal  
700 flux-states demonstrated that EcoTWIN is a transferable, flexible prediction and learning tool for  
701 process inference across biomes ranging from boreal to subtropical climate. Constrained by tracer  
702 simulations, the model not only reproduces the celerity of hydrological systems, but also tracks the  
703 velocity. Water ages and travel time are embedded in EcoTWIN to provides spatio-temporal-explicit  
704 insights into *when*, *where*, and *how* water moves in the system. Such indices further provide the  
705 opportunities to efficiently bridge hydrology and water quality at large catchment-scales. An example  
706 was presented using the Damköhler Number to identify regions where denitrification was limited by  
707 fast turnover rates of water.

708 Following this “proof of concept” we also see numerous areas where future developments can  
709 improve the limitations in the 1.0 version of the model.

710

## 711 **Code and data availability**

712 The initial version (v1.0) of EcoTWIN is archived in <https://doi.org/10.5281/zenodo.16747633> (Wu et  
713 al., 2025d). For further development please refer to GitHub repository: [https://github.com/songjun-  
714 wu/EcoTWIN](https://github.com/songjun-wu/EcoTWIN). The geographic data were acquired from Catchment Characterisation and Modelling  
715 database (CCM2, version 2.1). The climatic forcing was acquired from E-OBS database  
716 (<https://www.ecad.eu/download/ensembles/ensembles.php>). The LAI were acquired from MODIS  
717 database (<http://doi.org/10.5067/MODIS/MOD15A2H.006>). Long-term observation of discharge was  
718 acquired from GRDC (<https://grdc.bafg.de/>); in-stream isotopic observations were available from  
719 Wateriso database (<https://wateriso.utah.edu/waterisotopes/index.html>) and GNIR database



720 (<https://www.iaea.org/services/networks/gnir>); In-stream NO<sub>3</sub>-N concentration were acquired from  
721 global water quality database, GEMStat (<https://gemstat.org/>).

722

### 723 **Acknowledgements**

724 Tetzlaff's and Wu's contributions were partly funded through the WETSCAPES2.0 project (DFG  
725 TRR410/1 2025) and the Einstein Research Unit "Climate and Water under Change" from the Einstein  
726 Foundation Berlin and Berlin University Alliance (grant no. ERU-2020-609). Tetzlaff was also partly  
727 funded through Leibniz Excellence project ISOSCALE and received funding from the  
728 "Wasserressourcenpreis 2024" of the Rüdiger Kurt Bode-Foundation. This research was also  
729 supported by the BMBF (funding code 033W034A), which supported the IGB stable isotope Laboratory.  
730 Contributions from Soulsby were supported by Leibniz Association Germany in the project Wetland  
731 Restoration in Peatlands.

732

### 733 **Author contribution**

734 Conceptualization: SW, DT, YZ, CS

735 Data curation: SW

736 Methodology: SW

737 Software: SW

738 Visualization: SW

739 Supervision: DT, CS

740 Writing (original draft preparation): SW

741 Writing (review and editing): SW, DT, YZ, CS

742

### 743 **Reference**

744 Akbarzadeh, Z., Maavara, T., Slowinski, S., & Van Cappellen, P. (2019). Effects of Damming on River  
745 Nitrogen Fluxes: A Global Analysis. *Global Biogeochemical Cycles*, 33.  
746 <https://doi.org/10.1029/2019GB006222>

747 Ala-aho, P., Tetzlaff, D., Mcnamara, J., Laudon, H., & Kormos, P. (2017). Modeling the isotopic  
748 evolution of snowpack and snowmelt: Testing a spatially distributed parsimonious approach.  
749 *Water Resources Research*, 53. <https://doi.org/10.1002/2017WR020650>

750 Amato, M. T., & Giménez, D. (2024). Predicting monthly near-surface soil temperature from air  
751 temperature and the leaf area index. *Agricultural and Forest Meteorology*, 345, 109838.  
752 <https://doi.org/10.1016/j.agrformet.2023.109838>



- 753 Arnold, J., Moriasi, D., Gassman, P., Abbaspour, K., White, M., Srinivasan, R., et al. (2012). SWAT:  
754 Model use, calibration, and validation. *Transactions of the ASABE (American Society of*  
755 *Agricultural and Biological Engineers)*, 55. <https://doi.org/10.13031/2013.42256>
- 756 Bajracharya, A., Moghairib, M., Stadnyk, T., & Asadzadeh, M. (2023). Process based calibration of a  
757 continental-scale hydrological model using soil moisture and streamflow data. *Journal of*  
758 *Hydrology: Regional Studies*, 47, 101391. <https://doi.org/10.1016/j.ejrh.2023.101391>
- 759 Benettin, P., Bailey, S., Campbell, J., Green, M., Rinaldo, A., Likens, G., et al. (2015). Linking water age  
760 and solute dynamics in streamflow at the Hubbard Brook Experimental Forest, NH, USA.  
761 *Water Resources Research*, 51, n/a-n/a. <https://doi.org/10.1002/2015WR017552>
- 762 Beven, K. (2006). A manifesto for the equifinality thesis. *Journal of Hydrology*, 320(1–2), 18–36.  
763 <https://doi.org/10.1016/J.JHYDROL.2005.07.007>
- 764 Beven, K. (2015). Facets of uncertainty: Epistemic uncertainty, non-stationarity, likelihood, hypothesis  
765 testing, and communication. *Hydrological Sciences Journal*, 61, 150407155940006.  
766 <https://doi.org/10.1080/02626667.2015.1031761>
- 767 Birkel, C., & Soulsby, C. (2015). Advancing tracer-aided rainfall-runoff modelling: A review of progress,  
768 problems and unrealised potential. *Hydrological Processes*, 29(25), 5227–5240.  
769 <https://doi.org/10.1002/HYP.10594>
- 770 Birkel, C., Tetzlaff, D., & Dunn, S. (2011). Using time domain and geographic source tracers to  
771 conceptualize streamflow generation processes in lumped rainfall-runoff models. *Water*  
772 *Resources Research - WATER RESOUR RES*, 47. <https://doi.org/10.1029/2010WR009547>
- 773 Bonchkovskiy, A., & Osadcha, N. (2024). Modelling of the nutrient load in the Sula River basin using  
774 the MONERIS. *Physical Geography and Geomorphology*, 47, 7–20.  
775 <https://doi.org/10.17721/phgg.2024.3-4.01>
- 776 Condon, L., Kollet, S., Bierkens, M., Maxwell, R., Hill, M., Franssen, H.-J., et al. (2021). Global  
777 Groundwater Modeling and Monitoring: Opportunities and Challenges. *Water Resources*  
778 *Research*, 57. <https://doi.org/10.1029/2020WR029500>
- 779 Craig, H., Gordon, L. I., & Horibe, Y. (1964). Isotopic exchange effects in the evaporation of water: 1.  
780 Low-temperature experimental results. *Journal of Geophysical Research*, 68(17), 5079–5087.  
781 <https://doi.org/10.1029/JZ068I017P05079>
- 782 Dawson, T., & Ehleringer, J. (1991). Streamside trees that do not use stream water. *Nature*, 350, 335–  
783 337. <https://doi.org/10.1038/350335a0>
- 784 Dick, J. J., Tetzlaff, D., Birkel, C., & Soulsby, C. (2015). Modelling landscape controls on dissolved  
785 organic carbon sources and fluxes to streams. *Biogeochemistry*, 122(2–3), 361–374.  
786 <https://doi.org/10.1007/S10533-014-0046-3>
- 787 Eckersten, H., Jansson, P. E., & Johnsson, H. (1994). SOILN model – user’s manual 2nd edition, Division  
788 of Agricultural Hydrotechnics Communications, 94:4. Department of Soil Sciences, Swedish  
789 University of AgriculturalSciences, 58pp, Uppsala.



- 790 Efstratiadis, A., & Koutsoyiannis, D. (2010). One decade of multi-objective calibration approaches in  
791 hydrological modelling: A review. *Hydrological Sciences Journal*, 55(1), 58–78.  
792 <https://doi.org/10.1080/02626660903526292>
- 793 Godsey, S. E., Aas, W., Clair, T. A., de Wit, H. A., Fernandez, I. J., Kahl, J. S., et al. (2010). Generality of  
794 fractal  $1/f$  scaling in catchment tracer time series, and its implications for catchment travel  
795 time distributions. *Hydrological Processes*, 24(12), 1660–1671.  
796 <https://doi.org/10.1002/hyp.7677>
- 797 Good, S. P., Soderberg, K., Guan, K., King, E. G., Scanlon, T. M., & Caylor, K. K. (2014).  $\delta^2\text{H}$  isotopic flux  
798 partitioning of evapotranspiration over a grass field following a water pulse and subsequent  
799 dry down. *Water Resources Research*, 50(2), 1410–1432.  
800 <https://doi.org/10.1002/2013WR014333>
- 801 Grizzetti, B., Vigiak, O., Udias, A., Aloe, A., Zanni, M., Bouraoui, F., et al. (2021). How EU policies could  
802 reduce nutrient pollution in European inland and coastal waters. *Global Environmental*  
803 *Change*, 69, 102281. <https://doi.org/10.1016/j.gloenvcha.2021.102281>
- 804 Hooper, R., Stone, A., Christophersen, N., de Melo, E., & Seip, H. (1988). Assessing the Birkenes Model  
805 of Stream Acidification using a multi-signal calibration methodology. *Water Resources*  
806 *Research - WATER RESOUR RES*, 24, 1308–1316. <https://doi.org/10.1029/WR024i008p01308>
- 807 Horita, J., Rozanski, K., & Cohen, S. (2008). Isotope effects in the evaporation of water: A status report  
808 of the Craig-Gordon model. *Isotopes in Environmental and Health Studies*, 44, 23–49.  
809 <https://doi.org/10.1080/10256010801887174>
- 810 Hrachowitz, M., Savenije, H., Bogaard, T. A., Tetzlaff, D., & Soulsby, C. (2013). What can flux tracking  
811 teach us about water age distribution patterns and their temporal dynamics? *Hydrology and*  
812 *Earth System Sciences*, 17(2), 533–564. <https://doi.org/10.5194/HESS-17-533-2013>
- 813 Huijgevoort, M., Tetzlaff, D., & Sutanudjaja, E. (2016). Using high resolution tracer data to constrain  
814 water storage, flux and age estimates in a spatially distributed rainfall-runoff model.  
815 *Hydrological Processes*, 30. <https://doi.org/10.1002/hyp.10902>
- 816 Jasechko, S., Kirchner, J., Welker, J., & McDonnell, J. (2016). Substantial proportion of global  
817 streamflow less than three months old. *Nature Geoscience*, 9.  
818 <https://doi.org/10.1038/NGEO2636>
- 819 Jung, H., Tetzlaff, D., Birkel, C., & Soulsby, C. (2025). Recent Developments and Emerging Challenges  
820 in Tracer-Aided Modeling. *Wiley Interdisciplinary Reviews Water*, 12.  
821 <https://doi.org/10.1002/wat2.70015>
- 822 Kale, R., & Sahoo, B. (2011). Green-Ampt Infiltration Models for Varied Field Conditions: A Revisit.  
823 *Water Resources Management*, 25, 3505–3536. <https://doi.org/10.1007/s11269-011-9868-0>
- 824 Kumar, R., Samaniego, L., & Attinger, S. (2013). Implications of distributed hydrologic model  
825 parameterization on water fluxes at multiple scales and locations. *Water Resources Research*,  
826 49(1), 360–379. <https://doi.org/10.1029/2012WR012195>



- 827 Kuppel, S., Tetzlaff, D., Maneta, M., & Soulsby, C. (2018). ECH2O-iso 1.0: Water isotopes and age  
828 tracking in a process-based, distributed ecohydrological model. *Geoscientific Model*  
829 *Development*, 11, 3045–3069. <https://doi.org/10.5194/gmd-11-3045-2018>
- 830 Landgraf, J., Tetzlaff, D., Birkel, C., Stevenson, J., & Soulsby, C. (2023). Assessing land use effects on  
831 ecohydrological partitioning in the critical zone through isotope-aided modelling. *Earth*  
832 *Surface Processes and Landforms*, 48. <https://doi.org/10.1002/esp.5691>
- 833 Lindström, G., Pers, C., Rosberg, J., Strömquist, J., & Arheimer, B. (2010). Development and test of the  
834 HYPE (Hydrological Predictions for the Environment) model – A water quality model for  
835 different spatial scales. *Hydrology Research*, 41. <https://doi.org/10.2166/nh.2010.007>
- 836 Maneta, M. P., & Silverman, N. L. (2013). A spatially distributed model to simulate water, energy, and  
837 vegetation dynamics using information from regional climate models. *Earth Interactions*,  
838 17(11), 1–44. <https://doi.org/10.1175/2012EI000472.1>
- 839 McDonnell, J. (2014). The two water worlds hypothesis: Ecohydrological separation of water between  
840 streams and trees? *Wiley Interdisciplinary Reviews: Water*, 1.  
841 <https://doi.org/10.1002/wat2.1027>
- 842 McDonnell, J., & Beven, K. (2014). Debates on Water Resources: The future of hydrological sciences:  
843 A (common) path forward? A call to action aimed at understanding velocities, celerities and  
844 residence time distributions of the headwater hydrograph. *Water Resources Research*, 50.  
845 <https://doi.org/10.1002/2013WR015141>
- 846 Mcmillan, H., Araki, R., Bolotin, L., Kim, D.-H., Coxon, G., Clark, M., & Seibert, J. (2025). Global patterns  
847 in observed hydrologic processes. *Nature Water*, 3. [https://doi.org/10.1038/s44221-025-](https://doi.org/10.1038/s44221-025-00407-w)  
848 [00407-w](https://doi.org/10.1038/s44221-025-00407-w)
- 849 Mikayilov, F., Rouholahnejad Freund, E., Ashraf Vaghefi, S., Srinivasan, R., Yang, H., & Klöve, B. (2015).  
850 A continental-scale hydrology and water quality model for Europe: Calibration and uncertainty  
851 of a high-resolution large-scale SWAT model. *Journal of Hydrology*, 524.  
852 <https://doi.org/10.1016/j.jhydrol.2015.03.027>
- 853 Nan, Y., He, Z., Tian, F., Wei, Z., & Tian, L. (2021). Can we use precipitation isotope outputs of isotopic  
854 general circulation models to improve hydrological modeling in large mountainous  
855 catchments on the Tibetan Plateau? *Hydrology and Earth System Sciences*, 25(12), 6151–6172.  
856 <https://doi.org/10.5194/hess-25-6151-2021>
- 857 Neal, C., Christophersen, N., Neale, R., Smith, C., & Reynolds, B. (1988). Chloride in precipitation and  
858 streamwater for the upland catchment of River Severn, mid- Wales; some consequences for  
859 hydrochemical models. *Hydrological Processes*, 2, 155–165.  
860 <https://doi.org/10.1002/hyp.3360020206>
- 861 Nearing, G., Ruddell, B., Bennett, A., Prieto, C., & Gupta, H. (2020). Does Information Theory Provide  
862 a New Paradigm for Earth Science? Hypothesis Testing. *Water Resources Research*, 56.  
863 <https://doi.org/10.1029/2019WR024918>



- 864 Ocampo, C., Sivapalan, M., & Oldham, C. (2006). Hydrological connectivity of upland-riparian zones in  
865 agricultural catchments: Implications for runoff generation and nitrate transport. *Journal of*  
866 *Hydrology*, 331, 643–658. <https://doi.org/10.1016/j.jhydrol.2006.06.010>
- 867 Pechlivanidis, I., Jackson, B., Mcintyre, N., & Wheeler, H. (2011). Catchment scale hydrological  
868 modelling: A review of model types, calibration approaches and uncertainty analysis methods  
869 in the context of recent developments in technology and applications. *GlobalNEST*  
870 *International Journal*, 13, 193–214.
- 871 Pesántez, J., Birkel, C., Gaona, G., Arciniega-Esparza, S., Murray, D., Mosquera, G., et al. (2023).  
872 Spatially distributed tracer-aided modelling to explore DOC dynamics, hot spots and hot  
873 moments in a tropical mountain catchment. *Hydrological Processes*, 37, 1–15.  
874 <https://doi.org/10.1002/hyp.15020>
- 875 Rakovec, O., Kumar, R., Mai, J., Cuntz, M., Thober, S., Zink, M., et al. (2016). Multiscale and Multivariate  
876 Evaluation of Water Fluxes and States over European River Basins. *Journal of*  
877 *Hydrometeorology*, 17, 287–307. <https://doi.org/10.1175/JHM-D-15-0054.1>
- 878 Rakovec, O., Mizukami, N., Kumar, R., Newman, A., Thober, S., Wood, A., et al. (2019). Diagnostic  
879 Evaluation of Large-Domain Hydrologic Models Calibrated Across the Contiguous United  
880 States. *Journal of Geophysical Research: Atmospheres*, 124.  
881 <https://doi.org/10.1029/2019JD030767>
- 882 Remondi, F., Kirchner, J., Burlando, P., & Fatichi, S. (2018). Water Flux Tracking with A Distributed  
883 Hydrological Model to Quantify Controls on the Spatio-Temporal Variability of Transit Time  
884 Distributions. *Water Resources Research*, 54. <https://doi.org/10.1002/2017WR021689>
- 885 Samaniego, L., Kumar, R., & Attinger, S. (2010). Multiscale parameter regionalization of a grid-based  
886 hydrologic model at the mesoscale. *Water Resour. Res.*, 46.  
887 <https://doi.org/10.1029/2008WR007327>
- 888 Seybold, E., Dwivedi, R., Musselman, K., Kincaid, D., Schroth, A., Classen, A., et al. (2022). Winter runoff  
889 events pose an unquantified continental-scale risk of high wintertime nutrient export.  
890 *Environmental Research Letters*, 17, 104044. <https://doi.org/10.1088/1748-9326/ac8be5>
- 891 Šimůnek, J., Šejna, M., Saito, H., & Van Genuchten, M. T. (2013). *The HYDRUS-1D software package*  
892 *for simulating the one-dimensional movement of water, heat, and multiple solutes in variably-*  
893 *saturated media (Version 4.17)*. Department of Environmental Sciences University of Riverside  
894 California, California.
- 895 Skrzypek, G., Mydłowski, A., Dogramaci, S., Hedley, P., Gibson, J. J., & Grierson, P. F. (2015). Estimation  
896 of evaporative loss based on the stable isotope composition of water using Hydrocalculator.  
897 *Journal of Hydrology*, 523, 781–789. <https://doi.org/10.1016/J.JHYDROL.2015.02.010>
- 898 Smith, A., Tetzlaff, D., Kleine, L., Maneta, M., & Soulsby, C. (2021). Quantifying the effects of land use  
899 and model scale on water partitioning and water ages using tracer-aided ecohydrological  
900 models. *Hydrology and Earth System Sciences*, 25, 2239–2259. [https://doi.org/10.5194/hess-](https://doi.org/10.5194/hess-25-2239-2021)  
901 [25-2239-2021](https://doi.org/10.5194/hess-25-2239-2021)
- 902 Soulsby, C., Birkel, C., Geris, J., Dick, J., Tunaley, C., & Tetzlaff, D. (2015). Stream water age distributions  
903 controlled by storage dynamics and nonlinear hydrologic connectivity: Modeling with high-



- 904 resolution isotope data. *Water Resources Research*, 51(9), 7759–7776.  
905 <https://doi.org/10.1002/2015WR017888>
- 906 Sprenger, M., Stumpp, C., Weiler, M., Aeschbach, W., Allen, S., Benettin, P., et al. (2019). The  
907 Demographics of Water: A Review of Water Ages in the Critical Zone. *Reviews of Geophysics*,  
908 57. <https://doi.org/10.1029/2018RG000633>
- 909 Tetzlaff, D., Buttle, J., Carey, S. K., Mcguire, K., Laudon, H., & Soulsby, C. (2015). Tracer-based  
910 assessment of flow paths, storage and runoff generation in northern catchments: A review.  
911 *Hydrological Processes*, 29(16), 3475–3490. <https://doi.org/10.1002/HYP.10412>
- 912 Wang, J., Bouwman, A., Vilmin, L., Beusen, A., Hoek, W., Liu, X., & Middelburg, J. (2024). Global inland-  
913 water nitrogen cycling has accelerated in the Anthropocene. *Nature Water*, 2.  
914 <https://doi.org/10.1038/s44221-024-00282-x>
- 915 Wellen, C., Kamran-Disfani, A.-R., & Arhonditsis, G. (2015). Evaluation of the Current State of  
916 Distributed Watershed Nutrient Water Quality Modeling. *Environmental Science &  
917 Technology*, 49. <https://doi.org/10.1021/es5049557>
- 918 Wen, Y., Lin, J.-S., Plaza, F., & Liang, X. (2024). Roles of Hydrology and Transport Processes in  
919 Denitrification at Watershed Scale. *Water Resources Research*, 60, 1–24.  
920 <https://doi.org/10.1029/2023WR034971>
- 921 Winkler, K., Fuchs, R., Rounsevell, M., & Herold, M. (2021). Global land use changes are four times  
922 greater than previously estimated. *Nature Communications*, 12(1), 2501.  
923 <https://doi.org/10.1038/s41467-021-22702-2>
- 924 Wu, S., Tetzlaff, D., Yang, X., & Soulsby, C. (2022). Disentangling the influence of landscape  
925 characteristics, hydroclimatic variability and land management on surface water NO<sub>3</sub>-N  
926 dynamics: spatially distributed modelling over 30 years in a lowland mixed land use catchment.  
927 *Water Resources Research*, e2021WR030566. <https://doi.org/10.1029/2021WR030566>
- 928 Wu, S., Tetzlaff, D., Beven, K., & Soulsby, C. (2025a). DREAM(LoAX): Simultaneous Calibration and  
929 Diagnosis for Tracer-Aided Ecohydrological Models Under the Equifinality Thesis. *Water  
930 Resources Research*, 61, e2024WR038779. <https://doi.org/10.1029/2024WR038779>
- 931 Wu, S., Tetzlaff, D., Yang, X., Sauter, T., & Soulsby, C. (2025b). Hydrological Connectivity Dominates  
932 NO<sub>3</sub>-N Cycling in Complex Landscapes – Insights From Integration of Isotopes and Water  
933 Quality Modeling. *Water Resources Research*, 61. <https://doi.org/10.1029/2025WR040525>
- 934 Wu, S., Tetzlaff, D., & Soulsby, C. (2025c). Revising Common Approaches for Calibration: Insights From  
935 a 1-D Tracer-Aided Hydrological Model With High-Dimensional Parameters and Objectives.  
936 *Water Resources Research*, 61, e2024WR037656. <https://doi.org/10.1029/2024WR037656>
- 937 Wu, S., Tetzlaff, D., Zheng, Y., & Soulsby, C. (2025d). EcoTWIN v1.0 release.  
938 <https://doi.org/10.5281/zenodo.16747633>
- 939 Yang, C., Condon, L., & Maxwell, R. (2025). Unravelling groundwater–stream connections over the  
940 continental United States. *Nature Water*, 3. <https://doi.org/10.1038/s44221-024-00366-8>
- 941 Yang, X., Jomaa, S., Zink, M., Fleckenstein, J., Borchardt, D., & Rode, M. (2018). A New Fully Distributed  
942 Model of Nitrate Transport and Removal at Catchment Scale. *Water Resources Research*, 54.  
943 <https://doi.org/10.1029/2017WR022380>



- 944 Yang, X., Zhang, X., Graeber, D., Hensley, R., Jarvie, H., Lorke, A., et al. (2023a). Large-stream nitrate  
945 retention patterns shift during droughts: Seasonal to sub-daily insights from high-frequency  
946 data-model fusion. *Water Research*, 243, 120347.  
947 <https://doi.org/10.1016/j.watres.2023.120347>
- 948 Yang, X., Tetzlaff, D., Müller, C., Knöller, K., Borchardt, D., & Soulsby, C. (2023b). Upscaling Tracer-  
949 Aided Ecohydrological Modeling to Larger Catchments: Implications for Process  
950 Representation and Heterogeneity in Landscape Organization. *Water Resources Research*, 59,  
951 e2022WR033033. <https://doi.org/10.1029/2022WR033033>
- 952 Yang, X., Tetzlaff, D., Jin, J., Li, Q., Borchardt, D., & Soulsby, C. (2024). Linking terrestrial biogeochemical  
953 processes and water ages to catchment water quality: A new Damköhler analysis based on  
954 coupled modeling of isotope tracers and nitrate dynamics. *Water Research*, 262, 122118.  
955 <https://doi.org/10.1016/j.watres.2024.122118>
- 956 Zhang, Z., Chen, X., Cheng, Q.-B., Li, S.-L., Yue, F.-J., Peng, T., et al. (2020). Coupled hydrological and  
957 biogeochemical modelling of nitrogen transport in the karst critical zone. *Science of The Total  
958 Environment*, 732, 138902. <https://doi.org/10.1016/j.scitotenv.2020.138902>
- 959 Zhu, J., Jia, Y., Yu, G., Wang, Q., He, N., Chen, Z., et al. (2025). Changing patterns of global nitrogen  
960 deposition driven by socio-economic development. *Nature Communications*, 16(1), 46.  
961 <https://doi.org/10.1038/s41467-024-55606-y>
- 962